JOURNAL OF GEOPHYSICAL RESEARCH, VOL. 108, NO. B2, 2121, doi:10.1029/2001JB001653, 2003

Shear heating of a fluid-saturated slip-weakening dilatant fault zone 1. Limiting regimes

Dmitry I. Garagash
Department of Civil and Environmental Engineering, Clarkson University, Potsdam, New York, USA

John W. Rudnicki
Department of Civil and Environmental Engineering, Northwestern University, Evanston, Illinois, USA

Received 19 November 2001; revised 23 September 2002; accepted 14 November 2002; published 25 February 2003.

[1] The one-dimensional model of *Rudnicki and Chen* [1988] for a slip-weakening dilating fault is extended to include shear heating. Because inertia is not included, instability (a seismic event) corresponds to an unbounded slip rate. Shear heating tends to increase pore pressure and decrease the effective compressive stress and the resistance to slip and consequently tends to promote instability. However, the decrease of effective compressive stress also reduces the magnitude of shear heating. Consequently, in the absence of frictional weakening and dilation, there exists a steady solution for slip at the tectonic rate in which the pressure does not change and the shear heating is exactly balanced by heat flux from the fault zone. In the absence of shear heating, dilatancy tends to decrease pore pressure and inhibit instability; more rapid slip weakening promotes instability. Analysis of undrained, adiabatic slip (characteristic of rapid slip or hydraulically and thermally isolated faults) reveals that the interaction of these effects can cause increased slip weakening to be stabilizing and increased dilatancy to be destabilizing. These counterintuitive effects are due to the dependence of the shear heating on the total shear stress (not just its change). They occur for small thermal expansivity and for material parameters within a plausible range for 0–10 km depth. *INDEX TERMS:* 3210 Mathematical Geophysics: Modeling; 3299 Mathematical Geophysics: General or miscellaneous; 5104 Physical Properties of Rocks: Fracture and flow; 5134 Physical Properties of Rocks: Thermal properties; 7209 Seismology: Earthquake dynamics and mechanics; *KEYWORDS:* fault, slip, friction, frictional heating, dilatancy

Citation: Garagash, D. I., and J. W. Rudnicki, Shear heating of a fluid-saturated slip-weakening dilatant fault zone, 1, Limiting regimes, *J. Geophys. Res.*, *108*(B2), 2121, doi:10.1029/2001JB001653, 2003.

1. Introduction

[2] Coupling of shear deformation with changes in the temperature and pressure of pore fluid can affect the stability of slip in fault gouge zones. Alterations of pore fluid temperature and pressure arise from shear-induced dilatancy or compaction and shear heating. These effects are examined using an extension of the model proposed by *Rudnicki and Chen* [1988] to study the stabilizing effects of pore fluid pressure reductions due to dilatancy on frictional slip.

[3] The role of pore fluid pressure on fault slip and rock failure processes has been well documented by both laboratory [e.g., *Brace and Martin*, 1968] and field studies [e.g., *Raleigh et al.*, 1976]. In addition, direct observation of fluid outflows following seismic events [*Sibson*, 1981] and geologic observations of extensive dilatant fractures and mineralized vein systems near faults [*Sibson*, 1981, 1987, 1988] provide further evidence of the connection between fault slip and pore fluid processes. Several authors [*Byerlee*, 1990, 1993; *Rice*, 1992; *Sibson*, 1991; *Sleep and Blanpied*, 1992] have suggested that high (near lithostatic) pore pressures could resolve issues concerning low stress levels on the San Andreas fault and modulate episodic occurrence of earthquakes.

[4] One mechanism by which pore pressure affects the stability of slip on faults is coupling with inelastic volume deformation in response to shear. Laboratory work has documented volume changes accompanying frictional slip [*Teufel*, 1981] and shearing of simulated fault gouge [*Marone et al.*, 1990; *Marone and Kilgore*, 1993; *Lockner and Byerlee*, 1994]. If the volume deformation occurs rapidly, by comparison to the timescale of pore fluid mass diffusion, it can cause an alteration of the local pore pressure and, via the effective stress principle, an alteration of the resistance to inelastic shearing or frictional slip. In particular, dilation tends to cause a reduction of pore fluid pressure, an increase in effective compressive stress, and, hence, an increase in resistance. Compaction produces the opposite effect. Dilatant hardening is the cause of apparent deviations from effective stress principle observed by *Brace and Martin* [1968] and stabilization of failure in axisymmetric compression tests on Westerly granite [*Martin*, 1980]. More

0148-0227/03/2001JB001653$09.00

recently, experiments by *Lockner and Byerlee* [1994] demonstrated that pore pressure reductions caused by dilatancy in hydraulically isolated faults can inhibit or even suppress instability. Several models [*Rudnicki and Chen*, 1988; *Sleep and Blanpied*, 1992; *Segall and Rice*, 1995; *Chambon and Rudnicki*, 2001] have examined the effect of dilatancy on stabilizing and modifying the evolution of slip on fluid-saturated faults.

[5] Shear heating is another mechanism by which pore pressure affects the stability of slip. Temperature rise due to frictional heating causes thermal expansion of the pore fluid and, consequently, an increase of the pore pressure. An increase in pore pressure decreases the effective compressive stress and reduces the frictional resistance. Importantly, shear heating introduces a dependence on the ambient compressive stress level (rather than just on the stress drop) and, thus, introduces a depth dependence in addition to that of material or transport properties. Geological observations of extensive vein systems near faults are interpreted as evidence for hydraulic fracturing and, consequently, pore fluid pressure rise in excess of the least compressive stress [*Sibson*, 1981], which can be caused by shear heating. *Lachenbruch* [1980], *Raleigh and Evernden* [1981], and *Mase and Smith* [1987] have examined the effects of factors such as stress level, hydraulic and thermal diffusivities, fault zone width, event duration, dilation and compressibility, on shear heating. These studies were, however, kinematic. That is, they specified the slip rather than determining it by means of a fault constitutive relation in response to imposed remote loading. In addition, these models did not include the possibility of slip instability. Other studies of the role of shear heating in frictional instability include the studies of *Shaw* [1995], *Sleep* [1995], and *Vardoulakis* [2000].

[6] Here and in the companion paper (D. I. Garagash and J. W. Rudnicki, Shear heating of a fluid-saturated slip-weakening dilatant fault zone, 2, Quasi-drained regime, submitted to *Journal of Geophysical Research*, 2002, hereinafter referred to as Garagash and Rudnicki, submitted manuscript, 2002), we extend the model of *Rudnicki and Chen* [1988] to study in detail the interaction of dilatancy and thermal pressurization on slip instability. As noted above, dilatancy tends to stabilize slip; more severe slip weakening tends to promote instability. We will show, however, that the interaction between shear heating, slip weakening, and dilatancy can cause dilatancy to promote instability and more severe slip weakening to stabilize slip. These surprising effects are due to the dependence of shear heating on the absolute stress level, not just its change.

2. Problem Formulation

[7] Figure 1 shows the geometry of the problem and the loading: a crustal block of thickness 2ℓ contains a fault zone of thickness 2λ with $\lambda \ll \ell$. Because the geometry and loading are symmetric about $y = 0$, the dashed line in Figure 1, only the portion $y \geq 0$ is shown. The slab extends indefinitely in the other directions so that the problem is one dimensional. The crustal block is loaded at its top surface ($y = \ell + \lambda$) by a normal stress σ and a shear displacement $\delta_\ell(t)$ related to the constant tectonic strain rate $\dot{\gamma}_\ell$ by $\delta_\ell = \ell\dot{\gamma}_\ell t$. Because the problem is symmetric about $y = 0$, the fault slip is twice the shear displacement $\delta(t)$ at the boundary of the fault zone ($y = \lambda$) and fault dilatancy is twice the normal displacement $\lambda(t) - \lambda_o$ of the fault boundary, where $\lambda(0) = \lambda_o$ is the initial half thickness of the fault zone. Pore fluid pressure p and temperature θ at $y = \ell + \lambda$ are equal to their ambient values p_o and θ_o.

2.1. Stress Equilibrium

[8] The stresses developed in the fault/crustal block system are a shear stress τ, a normal stress σ, and whatever reaction stresses are needed to maintain zero deformation in planes perpendicular to the y direction. Because we neglect inertia and any spatial dependence is only on y, equilibrium requires that τ and σ be uniform throughout the layer. We measure time and slip on the fault from the point at which the shear stress is τ_o at a normal stress σ_o. The material in the fault zone ($0 \leq y \leq \lambda$) undergoes inelastic loading whereas the material in the crustal block ($\lambda < y \leq \ell + \lambda$) behaves elastically. Thus, the stress in the crustal block is given by elastic relation

$$\tau = \tau_o + G(\dot{\gamma}_\ell t - \delta/\ell) \tag{1}$$

where G is elastic modulus.

[9] The relation between the stress and slip in the fault zone is taken to have the simple form (which is explained in more detail by *Rudnicki and Chen* [1988])

$$\tau = \tau_o + \tau_{flt}(\delta) + \mu_o\left[\sigma' - \sigma'_o\right] \tag{2}$$

where $\tau_{flt}(\delta)$ (with $\tau_{flt}(0) = 0$) gives the slip dependence under constant effective normal stress $\sigma' = \sigma'_o$. The third term in (2) corresponds to the change in frictional resistance due to the changes in effective normal stress, $\sigma' = \sigma - p$, where σ is the total normal stress and p is the pore fluid pressure. The friction coefficient μ_o is assumed here to be constant but, may, in general, depend on effective normal stress, slip, slip history, temperature, and fluid pressure. Because equilibrium requires that the stress in the layer be uniform, expressions (1) and (2) must be equal

$$G(\dot{\gamma}_\ell t - \delta/\ell) = \tau_{flt}(\delta) + \mu_o\left[\sigma' - \sigma'_o\right] \tag{3}$$

2.2. Pore Fluid Flow

[10] Fluid mass conservation for the fault zone can be expressed as

$$\lambda_o\dot{\zeta} + q = 0 \tag{4}$$

where $\dot{\zeta}$ is the average volumetric rate of fluid content variation per unit reference volume (averaged over the thickness of the fault zone and q is the fluid exchange between the layer and the adjacent crustal block. (The superposed dot denotes the derivative with respect to time). For constant mean stress, the rate of fluid content variation $\dot{\zeta}$ can be expressed as [e.g., *Coussy*, 1995]

$$\dot{\zeta} = \frac{\dot{p}}{K'} - \beta'\dot{\theta} + \dot{\phi}^p \tag{5}$$

where θ is temperature, $\dot{\phi}^p$ is inelastic rate of change of porosity ϕ, K' is an effective fluid bulk modulus, and β' is the effective fluid thermal expansion coefficient. The effective bulk modulus K' can be expressed as follows in terms of the drained (constant pore pressure) bulk modulus K, the fluid

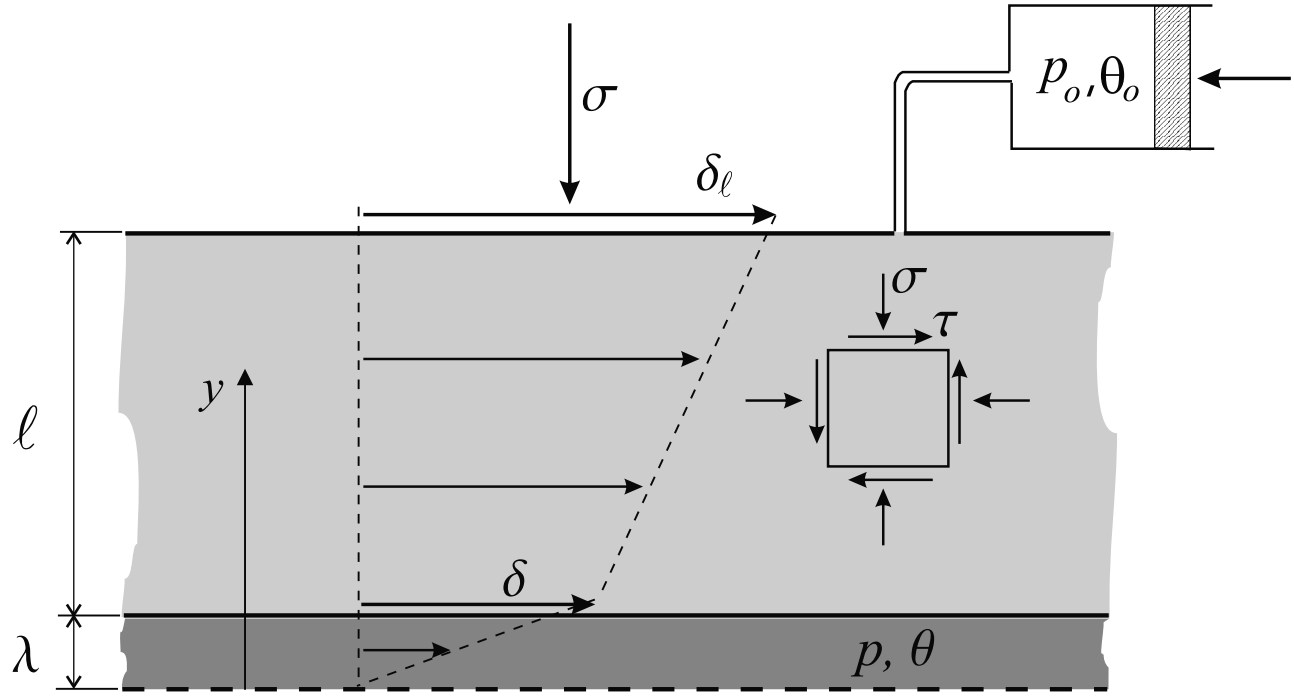

Figure 1. Sketch of the problem.

bulk modulus K_f and two additional bulk moduli K_s' and K_s'' [*Rice and Cleary*, 1976; *Detournay and Cheng*, 1993]

$$\frac{1}{K'} = \frac{1}{K} - \frac{1}{K_s'} + \frac{\phi_o}{K_f} - \frac{\phi_o}{K_s''} \tag{6}$$

where ϕ_o is initial porosity. Similarly, β' can be expressed as [*McTigue*, 1986; *Coussy*, 1995]

$$\beta' = \phi_o(\beta_f - \beta_s) \tag{7}$$

where β_f and β_s are the expansion coefficients of the fluid and solid constituents, respectively.

[11] Slip on the fault is accompanied by inelastic changes in porosity ϕ^p. Although, in general, compaction ($\dot{\phi}^p < 0$) is possible, porosity changes due to slip on frictional surfaces or well-consolidated fault zones appear to be primarily dilatant. Dilation may be due to a variety of processes, such as microcrack opening in or near the fault zone, uplift in sliding over asperity contacts, or grain rearrangement. As noted by *Rudnicki and Chen* [1988], dilation that is a simple, nondecreasing function of the slip $\phi^p = \phi^p(\delta)$ is consistent with experiments.

[12] According to Darcy's law, fluid flux q is proportional to the negative of the pore pressure gradient, but following the studies of *Rudnicki and Chen* [1988] and *Segall and Rice* [1995], we simplify this relation in a manner consistent with the one degree of freedom approximation used here. In particular, the fluid flux from the fault zone is assumed to be proportional to the difference of fault zone pressure p and the remote far-field ambient pressure, p_o,

$$q \simeq \kappa \frac{p - p_o}{\ell_\kappa} \tag{8}$$

where ℓ_κ is a length scale that has to be chosen to reflect pore fluid diffusion on the timescale of interest. This diffusion length ℓ_κ is bounded by the crustal block thickness ℓ and, presumably, much larger than fault half thickness λ, at least if slip rates are not too high. An implication of the approximation (8) is that the pore fluid pressure is uniform in the fault zone. This is reasonable if the fault zone is composed of gouge (crushed rock) with permeability much higher than the intact rock in the adjacent crustal block. Substituting (5) and (8) into (4) yields a fluid continuity equation for the slip layer

$$\dot{\phi}^p + \frac{\dot{p}}{K'} - \beta'\dot{\theta} = -\kappa \frac{p - p_o}{\lambda_o \ell_\kappa} \tag{9}$$

2.3. Energy Conservation

[13] In a manner similar to (4), energy conservation for the fluid-infiltrated fault zone layer, averaged through the half thickness λ, can be expressed as

$$\lambda_o C\dot{\theta} = -Q + \Psi^p \tag{10}$$

where $\dot{\theta}$ is the rate of temperature change, C is heat capacity of the gouge, Q is the heat flux at the slip layer boundary, $y = \lambda$, and Ψ^p is the thickness averaged rate of mechanical energy dissipation due to inelastic deformation. This form of the energy balance neglects contributions to the rate of energy storage from elastic strain of the solid skeleton and pore pressure changes by comparison with the thermal heat storage $C\dot{\theta}$ [*McTigue*, 1986; *Coussy*, 1995].

[14] The thickness averaged rate of mechanical energy dissipation is given by

$$\Psi^p = \tau\dot{\delta} \tag{11}$$

In general, there may be an additional term from the product of the effective normal stress and the thickness change.

Because the ratio of dilation (or compaction) to slip is small, this term is negligible by comparison with $\tau\dot{\delta}$. The heat flux Q, which satisfies Fourier's law, is approximated in the same way as the fluid flux (8)

$$Q \simeq \chi \frac{\theta - \theta_o}{\ell_\chi} \tag{12}$$

where χ is thermal conductivity of the crustal rock and ℓ_χ is the lumped parameter (analogous to ℓ_κ in (8)) which characterizes the thermal diffusion length for timescale of interest. Substituting (11) and (12) into (10) yields the form of the energy conservation for the slip layer

$$\lambda_o C\dot{\theta} = \tau\dot{\delta} - \chi \frac{\theta - \theta_o}{\ell_\chi} \tag{13}$$

2.4. Qualitative Discussion of Slip Governing Equations

[15] The evolution of slip on the fault is governed by (3), (9), and (13). In this subsection, we rearrange these equations to illustrate the main effects that will be discussed in more detail in the remainder of the paper.

[16] Differentiating (3) with respect to time and assuming constant total normal stress $\sigma = \sigma_o$, yields

$$\left[\frac{G}{\ell} + \frac{d\tau_{flt}}{d\delta}\right]\dot{\delta} = G\dot{\gamma}_\ell + \mu_o\dot{p} \tag{14}$$

If the pore fluid pressure is constant, then the slip rate $\dot{\delta}$ is simply proportional to the imposed strain rate $\dot{\gamma}_\ell$ with the proportionality factor depending on the fault stress versus slip relation. As long as $d\tau_{flt}/d\delta$ is positive (slip strengthening) or not so negative (slip weakening) that the square bracket multiplying the slip rate in (14) becomes negative, the slip rate will be positive and finite. As $d\tau_{flt}/d\delta$ becomes more negative, the value of the bracket decreases and the ratio of the fault slip rate $\dot{\delta}$ to the imposed strain rate $\dot{\gamma}_\ell$ becomes large. This ratio becomes unbounded if $d\tau_{flt}/d\delta$ is sufficiently negative as to equal $-G/\ell$ and the coefficient of $\dot{\delta}$ in (14) is zero. This corresponds to an unstable, dynamic slip event. In other words, an inertial instability occurs when the stress on the fault decreases faster due to slip than the adjacent material can unload elastically. If we had not neglected inertia or included a damping term [*Rice*, 1993; *Segall and Rice*, 1995], the slip rate would become large (of the order of wave speeds) but not unbounded. Equation (14) shows that an increase in pore fluid pressure ($\dot{p} > 0$) increases the slip rate and a decrease ($\dot{p} < 0$) decreases the slip rate.

[17] Using (13) to eliminate the temperature rate $\dot{\theta}$ from (9) yields an expression for the rate of change of pore pressure:

$$\dot{p} = K'\left[\frac{\beta'\tau}{\lambda_o C} - \frac{d\phi^p}{d\delta}\right]\dot{\delta} - \frac{1}{t_\kappa}(p - p_o) - \frac{K'\beta'}{t_\chi}(\theta - \theta_o) \tag{15}$$

where $t_\kappa = \lambda_o\ell_\kappa/\kappa K'$ and $t_\chi = \lambda_o\ell_\chi C/\chi$ are timescales of pore fluid and thermal diffusion, respectively. If both t_κ and t_χ are large (undrained, adiabatic conditions), then the last two terms in (15) can be neglected. Because $K'\dot{\delta}$ is positive, the sign of the pore pressure change is governed by the sign of the quantity in the square bracket. The first term $\beta'\tau/\lambda_o C$ reflects the tendency of shear heating to increase the pore pressure; the second term $d\phi^p/d\delta$ will also tend to increase the pore pressure if negative (compaction) but tends to decrease it if positive (dilation). Note, however, that the shear stress τ also depends on the pore pressure through the effective normal stress (2) and is decreased by increasing pore pressure. Thus, pore pressure increases caused by shear heating will tend to diminish the rate of pore pressure change. Solutions developed later will demonstrate the importance of this effect.

[18] Substitution of (15) into (14) yields

$$\left[\frac{G}{\ell} + \frac{d\tau_{flt}}{d\delta} - \frac{\mu_o K'\beta'\tau}{\lambda_o C} + \mu_o K'\frac{d\phi^p}{d\delta}\right]\dot{\delta} = G\dot{\gamma}_\ell - \frac{\mu_o}{t_\kappa}(p - p_o) - \frac{\mu_o K'\beta'}{t_\chi}(\theta - \theta_o) \tag{16}$$

As discussed in connection with (15), the last two terms reflect the contributions of fluid mass flux and heat conduction and, as discussed in connection with (14), the vanishing of the coefficient of $\dot{\delta}$ corresponds to the onset of an inertial instability. Because the slip rate must be positive and the right-hand side of (16) is initially positive ($p = p_o$ and $\theta = \theta_o$), the term in square brackets multiplying the slip rate must also be positive initially. If not, slip is inherently unstable or the point of instability has already been passed in the slip history. *Rudnicki and Chen* [1988] began their calculations at peak stress on the fault, $d\tau_{flt}/d\delta = 0$, assumed dilation ($d\phi^p/d\delta > 0$) and neglected thermal coupling ($\beta' = 0$). Consequently, the slip rate was initially positive and remained so until instability. When thermal coupling is included ($\beta' \neq 0$), it is possible that the bracket multiplying $\dot{\delta}$ is initially negative unless either or both $d\tau_{flt}/d\delta$ and $d\phi^p/d\delta$ are positive (slip hardening and dilation) and sufficiently large. Here we also begin calculations at peak stress. As a result the requirement of an initially positive slip rate introduces the following restriction

$$\left[\frac{G}{\ell} - \frac{\mu_o K'\beta'\tau}{\lambda_o C} + \mu_o K'\frac{d\phi^p}{d\delta}\right]_{\delta=0} > 0 \tag{17}$$

Alternatively, we could view the requirement of initially positive slip rate as restricting the initial value of $d\tau_{flt}/d\delta$ to be sufficiently positive (slip strengthening).

2.5. Particular Form of τ_{flt} and ϕ^p

[19] To complete the formulation, we adopt particular forms of shear resistance slip dependence ($\tau_{flt}(\delta)$) and fault dilation ($\phi^p(\delta)$) used by *Rudnicki and Chen* [1988]. The shear resistance is given by:

$$\tau_{flt} = -(\tau_o - \tau_r)g(\delta/\delta_r) \tag{18}$$

where τ_o and τ_r ($\tau_r < \tau_o$) are initial peak shear stress and residual shear stress (under constant effective normal loading $\sigma' = \sigma'_o$), respectively. The function $g(\delta/\delta_r)$ describes the decrease of τ from τ_o to τ_r over the slip distance δ_r (Figure 2a), i.e., $g(0) = 0$ and $g(1) = 1$. The inelastic change of porosity is

$$\phi^p = \phi^p_r f(\delta/\delta_r) \tag{19}$$

where the function f increases from zero to unity as its argument increases from zero to unity, corresponding to an inelastic increase of the porosity from zero to ϕ^p_r over the slip distance δ_r (see Figure 2b).

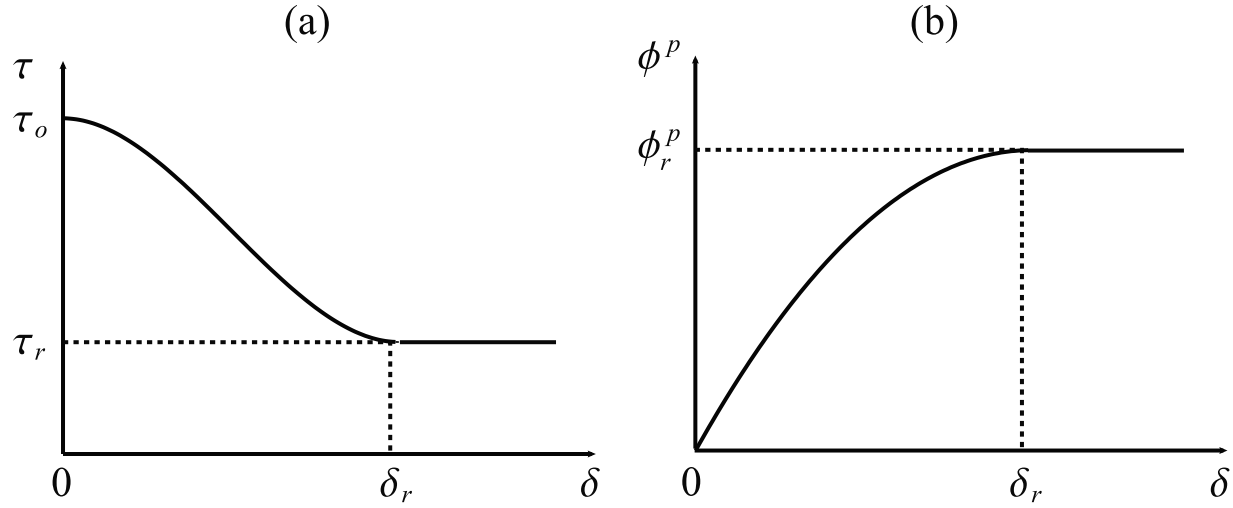

Figure 2. Fault constitutive relations: (a) decrease of shear stress τ on the fault with the slip δ under constant effective normal stress ($\sigma' = \sigma'_o$) (2) and (b) fault gauge dilation: inelastic changes in porosity ϕ^p with the slip δ (19).

[20] Although the relation (19) has the same form as that of *Rudnicki and Chen* [1988, equation (5)], they expressed the dilation directly in terms of fault opening. Because the opening was zero at the initiation of slip, the initial normal strain rate was unbounded. As a consequence, so was the initial pressure decrease for undrained deformation and undrained deformation was always stable. The present formulation removes this unrealistic feature, though at the expense of requiring specification of the initial fault zone width.

3. Normalized Equations

[21] The relevant timescales and relative magnitudes of various parameters for in situ applications are most easily determined by writing the equations in nondimensional form. To do so, a characteristic slip time t_s, pressure p_*, and temperature θ_* are defined as follows:

$$t_s = \frac{\delta_r}{\dot{\gamma}_\ell \ell},\ p_* = \frac{G}{\mu_o}\frac{\delta_r}{\ell},\ \theta_* = \frac{p_*}{C}\frac{\delta_r}{\lambda_o} \tag{20}$$

in addition to the characteristic times for pore fluid and thermal diffusion defined following (15). Using these, the dimensionless time T, slip Δ, stress Σ_τ, pressure change Π and temperature change Θ are given by

$$T = \frac{t}{t_s},\ \Delta = \frac{\delta}{\delta_r},\ \Sigma_\tau = \frac{\tau}{p_*},\ \Pi = \frac{p - p_o}{p_*}, \Theta = \frac{\theta - \theta_o}{\theta_*} \tag{21}$$

Equations (9), (3), and (13) can then be written in the dimensionless form

$$T - \Delta + \frac{2}{3}\mathcal{A}g(\Delta) = -\Pi \tag{22}$$

$$\Phi f'(\Delta)\dot{\Delta} + \dot{\Pi} - \mathcal{B}\dot{\Theta} = -\frac{1}{\epsilon}\Pi \tag{23}$$

$$\dot{\Theta} - \Sigma_\tau \dot{\Delta} = -\frac{1}{\epsilon_\chi}\ \Theta \tag{24}$$

where the superposed dot now denotes the derivative with respect to the nondimensional time T and the expression for dimensionless shear stress Σ_τ is given by

$$\Sigma_\tau = \Sigma_\tau^o + \mu_o(T - \Delta) \tag{25}$$

The coefficients in these equations are the following six dimensionless parameters:

$$\epsilon = \frac{t_\kappa}{t_s},\ \epsilon_\chi = \frac{t_\chi}{t_s},\ \Phi = \frac{\phi_r^p}{p_*(K')^{-1}},$$
$$\mathcal{B} = \frac{\theta_*\beta'}{p_*(K')^{-1}},\ \mathcal{A} = \frac{3}{2}\frac{\tau_o - \tau_r}{\mu_o p_*},\ \Sigma_\tau^o = \frac{\tau_o}{p_*}, \tag{26}$$

where

1. ϵ is the ratio of the timescale for pore fluid diffusion to that of imposed strain
2. ϵ_χ is the ratio of the timescale for heat fluid diffusion to that of imposed strain;
3. Φ is a measure of residual fault inelastic dilation relative to pore fluid compressibility;
4. $\mathcal{B}$ is a measure of the thermal expansivity of the pore fluid relative to the pore fluid compressibility;
5. $\mathcal{A}$ is a measure of frictional stress drop in the course of the slip; and
6. Σ_τ^o is a measure of peak shear stress, which quantifies the absolute shear stress level.

[22] The case $\epsilon \ll 1$ ($\epsilon_\chi \ll 1$) corresponds to "drained" ("isothermal") conditions: diffusion of pore fluid between the fault and its surroundings (heat exchange) occurs rapidly compared with the timescale of slip. Therefore, there is no change in the pore pressure (temperature), $\Pi = 0$ ($\Theta = 0$), in this limit. The case of $\epsilon \gg 1$ ($\epsilon_\chi \gg 1$) corresponds to the "undrained" ("adiabatic") slip regime. In this regime, pore fluid diffusion (heat exchange) is very slow on the timescale of the slip, and, therefore, can be neglected.

[23] Substituting the expressions for Π (22) and $\dot{\Theta}$(24) into (23) and combining the result with (24) yields a system

of two ordinary differential equations for the normalized slip Δ and temperature difference Θ

$$\dot{\Delta} = \frac{1}{\epsilon}\frac{N(T,\Delta,\Theta)}{D(T,\Delta)} \tag{27}$$

$$\dot{\Theta} = \Sigma_\tau \dot{\Delta} - \frac{1}{\epsilon_\chi}\Theta \tag{28}$$

The numerator N and denominator D on the right-hand side of (27) are specified by

$$N = -\Pi + \epsilon\left(1 - \frac{\mathcal{B}}{\epsilon_\chi}\Theta\right) \tag{29}$$

$$D = \Phi f'(\Delta) + 1 - \frac{2}{3}\mathcal{A}g'(\Delta) - \mathcal{B}\Sigma_\tau, \tag{30}$$

where the pressure Π and shear stress Σ_τ are functions of T and Δ given by (22) and (25), respectively. In terms of the nondimensional parameters, the requirement of initially positive slip rate (17) becomes

$$2\Phi + 1 - \mathcal{B}\Sigma_\tau^o > 0 \tag{31}$$

where we have used $f'(0) = 2$ for the form of the dilatancy function used in the calculations (see (A1) in Appendix A). This condition can be expressed as a requirement that the dilatancy must exceed a minimum value given by

$$\Phi_{\min} = -\frac{1 - \mathcal{B}\Sigma_\tau^o}{2} \tag{32}$$

[24] Slip instability corresponding to an unbounded slip rate ($\dot{\Delta} \to \infty$) occurs when the denominator of (27) $D(T, \Delta)$ vanishes but the numerator $N(T, \Delta, \Theta)$ does not. The instability corresponds to the onset of dynamic slip and earthquake nucleation. Stick ($\dot{\Delta} = 0$) is also a possibility if the numerator of (27) vanishes when the denominator does not.

4. Typical Values of the Problem Parameters

[25] The model, despite its simplicity, contains a number of material, geometric and loading parameters, but, as discussed above, these enter a smaller set of nondimensional groups. Although the model is simple enough that it is possible to evaluate the response for a wide range of parameters, we constrain that range to a realistic variation for faults in situ. This section discusses the numerical values of dimensional parameters, corresponding values of dimensionless constants governing the solution, and the variation of some of the relevant parameters with depth. For the most part, we choose mechanical and hydraulic parameters consistent with those used by *Rudnicki and Chen* [1988] and *Segall and Rice* [1995] and thermal parameters similar to those of *Lachenbruch* [1980] and *Mase and Smith* [1987].

4.1. Dimensional Parameters

[26] Following the study of *Rudnicki and Chen* [1988], we take $G = 30$ GPa, $\kappa G = 0.1$ m^2 s^{-1}, $\mu_o = 0.6$, $\delta_r = 0.1$ m, $\tau_o - \tau_r \approx 10$ MPa, $\dot{\gamma}^\ell \sim 10^{-15}$ s^{-1} as representative in situ values for the crustal shear modulus, effective fluid mobility (diffusivity), friction coefficient, residual slip distance, frictional stress drop, and tectonic shear strain rate, respectively. As *Rudnicki and Chen* [1988] discuss in more detail, in situ values of the diffusivity vary over several orders of magnitude. A number of observations suggest that the value 0.1 m^2 s^{-1} is reasonable near active faults but values an order of magnitude larger or smaller are widely observed. Similarly, the residual sliding distance is poorly constrained by observations. The value used here is considerably larger than values determined from laboratory specimens in order to reflect the larger-scale fault roughness and inhomogeneity that exists in the field.

[27] Consider the thermal properties of the gouge material. *Lachenbruch* [1980] gives a value of 0.24 cal (g°C)$^{-1}$ for the specific heat (per unit mass) of gouge. (*Mase and Smith* [1987] use an equivalent value in different units.) Multiplying by a typical rock density, 2.7 g cm^{-3}, yields a value for the specific heat (per unit volume) of gouge $C \sim 3$ MPa °C^{-1}. *Lachenbruch* [1980] cites the range of (0.7–1.2) $\times$ 10^{-2} cm^2 s^{-1} as reasonable for thermal diffusivities of gouge zone material but suggests that the lower value is more appropriate for disaggregated material. *Mase and Smith* [1987] use a value comparable to the lower end of the range given by *Lachenbruch* [1980] (6.65 $\times$ 10^{-3} cm^2 s^{-1}). The thermal diffusivity corresponds here to the ratio χ/C. Thus, multiplying the lower end value of *Mase and Smith* [1987] by $C = 3$ MPa °C^{-1} yields $\chi = 2N/s$°C.

[28] The choice of the length ℓ is inevitably uncertain since it arises from approximating a fault in a continuum as a one degree of freedom, spring-mass system but *Rudnicki and Chen* [1988] suggest values in the range of $\ell \sim 10^2$ to 10^3 m. Values of the fault thickness in the range $\lambda_o \sim 10^{-2}$ to 1 m, are reasonable. *Chester et al.* [1993] report values of about 0.1 m for a portion of the San Andreas fault. Values much smaller than 1 cm are not feasible and, on the other hand, values much larger than 1 m would contradict the view of a fault as a zone of localized deformation.

[29] The residual value of the inelastic porosity ϕ_r^p is taken to be in the range 10^{-4} to 10^{-2}. This range is consistent with that estimated by *Rudnicki and Chen* [1988] (their Δ_o/δ_o) from laboratory experiments of *Teufel* [1981] and with values of the dilatancy parameter used by *Segall and Rice* [1995] (their ϵ).

[30] The pore fluid compressibility K_f^{-1} and thermal expansivity β_f that enter the effective compressibility $(K')^{-1}$(6) and expansivity β' (7) are functions of the pressure and temperature and, hence, will evolve with the slip. The magnitude of the changes is, however, likely to be small compared with values at the ambient pressure and temperature. The solutions to be presented generally support this supposition although very near instability or for hydraulically or thermally isolated faults, the changes can be sufficiently large that they should be included in a more elaborate model. We do, however, include variations of K_f^{-1} and β_f with depth because of variations of the ambient pressure p_o and temperature θ_o. Assuming hydrostatic conditions, the pore pressure gradient is about 10 MPa km^{-1} and a representative geothermal gradient is 20–25°C km^{-1} [e.g., *Henyey and Wasserburg*, 1971; *Lachenbruch and Sass*, 1973]. Assuming the pore fluid is liquid water, we

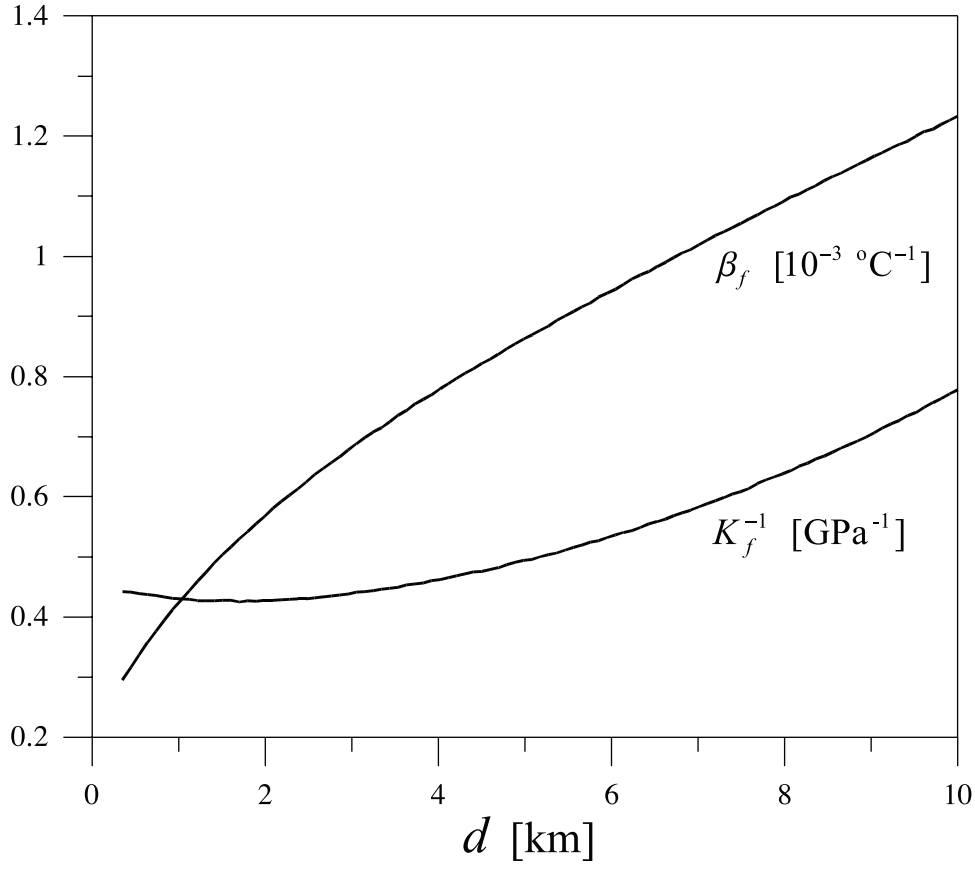

Figure 3. Plot of ambient K_f^{-1} and β_f versus depth d (assuming existing water properties data [*Wagner and Kruse*, 1998] and that ambient fluid pressure and temperature vary along hydrostatic and geothermal gradients).

can calculate the variation of K_f^{-1} and β_f with depth from these gradients using existing water property data (Figure 3) [e.g., *Wagner and Kruse*, 1998]. The fluid compressibility K_f^{-1} varies by a factor of 2, from approximately 0.4 to 0.8 GPa^{-1} and the expansivity β_f varies by one order of magnitude from about 10^{-4} to 10^{-3} °C^{-1} over the depth range of 0–10 km (Figure 3).

[31] For the values of the initial gouge zone porosity ϕ_o and the bulk modulus K, we take those used by *Segall and Rice* [1995] in their simulations: $\phi_o = 0.05$ and $K = 2$ GPa (K corresponds to β^{-1} of *Segall and Rice* [1995]). They suggest these values are appropriate estimates for gouge zone properties at seismogenic depths that are consistent with laboratory experiments. For these values K^{-1} in (6) exceeds $\phi_o K_f^{-1}$ by at least one order of magnitude and if, in addition, $K^{-1} \gg \phi_o K'_s$, $\phi_o K''_s$, as is likely for gouge zone material, then $K' \approx K$ follows from (6). *Mase and Smith* [1987] give $\beta_s = 2 \times 10^{-5}$ °C^{-1}. Using this value with $\phi_o = 0.05$ and β_f in the range 10^{-4} to 10^{-3} °C^{-1} in (7) yields $\beta' \approx \phi_o \beta_f$, with values ranging from 5×10^{-6} to 5×10^{-5} °C^{-1}.

[32] The normal stress σ_o is assumed to be constant during slip but variation with depth according to the lithostatic gradient is included. As discussed by *Chambon and Rudnicki* [2001], alterations of normal stress by slip on planar faults are generally small except near the free surface. For a lithostatic gradient of approximately 30 MPa km^{-1} and a hydrostatic variation of pore pressure with depth of 10 MPa km^{-1}, the gradient of residual shear stress $\tau_r = \mu_o(\sigma_o - p_o)$ is estimated as 10 MPa km^{-1}. If the frictional stress drop, $\tau_o - \tau_r \approx 10$ MPa, is independent of depth, then the peak stress is calculated to be $\tau_o = 10 + 12d$ MPa, where d is the depth in kilometers. Although it might be expected that the stress drop $\tau_o - \tau_r$ also decreases with depth as conditions change from brittle to more ductile, we take it as a constant. As discussed by *Rudnicki and Chen* [1988], there is some evidence from laboratory tests that the stress drop decreases with increasing confining stress but the observed decrease is small. In addition, stress drops inferred seismically show little systematic depth variation although seismic stress drops do not correspond directly to the frictional stress drop $\tau_o - \tau_r$.

4.2. Scaling and the Values of Dimensionless Parameters

[33] Using the estimates above we can calculate the characteristic pressure p_* and temperature $\theta_*(20)$ and the nondimensional parameters (26) ϵ, ϵ_χ, Φ, $\mathcal{B}$, $\mathcal{A}$, and Σ_τ^o. Using $G = 30$ GPa, $\mu_o = 0.6$, $\delta_r = 0.1$ m and crustal block thickness $\ell = 10^3$ m yields $p_* = 5$ MPa. Using this value of p_*, $C = 3$ MPa °C^{-1}, and $\lambda_o = 0.1$ m yields $\theta_* = 1.7$°C. Both the values of p_* and θ_* are an order of magnitude larger for the smaller estimate of the crustal block thickness $\ell = 10^2$ m.

[34] Because the characteristic temperature θ_* depends inversely on the fault zone thickness, λ_o, θ_* may be an order of magnitude larger (17°C) or smaller (0.17°C) for the range

of fault zone thicknesses cited above, 10^{-2} to 1 m. Several authors [*Lachenbruch*, 1980; *Cardwell et al.*, 1978; *Mase and Smith*, 1987] have noted the strong dependence of predictions of fault zone temperature rises on the assumptions about the (poorly constrained) fault zone width. To some extent, this strong dependence results from the appearance of the volumetric heat capacity C in (20). An alternative interpretation is to regard the product $C\lambda_o$ as an effective heat capacity for the fault surface. Although this might seem simply to exchange uncertainty about fault width for uncertainty about the product $C\lambda_o$, this product can be regarded as possessing a finite limit as the fault zone width goes to zero and, hence, does not exhibit the pathology resulting from taking λ_o very small with C finite.

[35] Using $p_* = 5$ MPa with $K' = 2.0$ GPa and a value for the residual inelastic porosity in the middle of the range cited above, $\phi_r^p = 10^{-3}$, yields $\Phi = 0.4$. The value of Φ could be an order of magnitude larger or smaller for the cited range of ϕ_r^p and an order of magnitude smaller for $\ell = 10^2$ m. For the same value of p_* and 10 MPa for the frictional stress drop $\tau_o - \tau_r$ (with $\mu_o = 0.6$), $\mathcal{A} = 5$. *Rudnicki and Chen* [1988] argue that, generally, $\mathcal{A}$ is of order unity for admissible crustal block thickness variations ℓ of the order of 10^2 to 10^3 m.

[36] The ratio ϵ/ϵ_χ is a characteristic velocity for heat transfer divided by that for fluid transfer:

$$\frac{\epsilon}{\epsilon_\chi} = \frac{\ell_\kappa(\chi/C)}{\ell_\chi(\kappa G)}\frac{G}{K'} \tag{33}$$

The fluid diffusivity $\kappa G = 10^3$ cm^2 s^{-1} exceeds by five orders of magnitude the range of thermal diffusivity χ/C suggested by *Lachenbruch* [1980], $(0.7–1.2) \times 10^{-2}$ cm^2 s^{-1}. Hence, for $G = 30$ GPa and $K' = 2$ GPa, as suggested in the preceding subsection, ϵ will be much less than ϵ_χ unless ℓ_κ exceeds ℓ_χ by four orders of magnitude. Given the small ratio of thermal to fluid diffusivity, this seems very unlikely. Both of the timescale ratios ϵ and ϵ_χ are proportional to the tectonic strain rate $\dot{\gamma}^\ell$, the product $\lambda_0\ell$ and either ℓ_κ (for ϵ) or ℓ_χ (for ϵ_χ). Since both ℓ_κ and ℓ_χ must be bounded by ℓ, setting $\ell_\kappa \approx \ell_\chi \approx \ell$ yields upper estimates for ϵ and ϵ_χ. Using ranges of λ_0 (10^{-2} to 1 m) and ℓ (10^2 to 10^3 m) and values of the other parameters discussed in the preceding subsection, yields

$$\epsilon \sim 10^{-10} \text{ to } 10^{-6},\ \epsilon_\chi \sim 10^{-6} \text{ to } 10^{-2} \tag{34}$$

Although the estimates vary over four orders of magnitude, both ϵ and ϵ_χ are much less than one and selecting values of ℓ_κ and ℓ_χ less than ℓ only reduces their magnitude. Since ℓ_κ and ℓ_χ appear only in ϵ and ϵ_χ, the analysis does not depend at all on their particular values (so long as they do not greatly exceed ℓ). Furthermore, despite the uncertainty in individual parameters entering ϵ and ϵ_χ, their magnitudes are certainly small. Consequently, conditions in the fault zone will be nearly drained ($\epsilon \ll 1$) and isothermal ($\epsilon_\chi \ll 1$) for much of its history. This, of course, is consistent with the notion that the timescale of tectonic straining is much longer than those for heat and fluid mass transfer (unless the fault is thermally and hydraulically isolated, a case we examine in section 5.3). The analysis of the companion paper (Garagash and Rudnicki, submitted manuscript, 2002) exploits the smallness of ϵ and ϵ_χ.

[37] For $p_* = 5$ MPa and $\tau_o = 10 + 12d$ MPa, where d is the depth in kilometers, as discussed above, the dimensionless peak stress is

$$\Sigma_\tau^o = 2 + 2.4d \tag{35}$$

The dimensionless thermal expansion $\mathcal{B}$(26) is given by

$$\mathcal{B} = \frac{\theta_*\phi_o\beta_f}{p_*/K'} = 20\,\theta_*\beta_f \tag{36}$$

where θ_* is in the range between 17°C ($\lambda_o = 1$ cm) and 0.17°C ($\lambda_o = 1$ m) and the thermal expansion coefficient β_f [°C^{-1}] is a function of depth. For a depth of the slip of 8 km, $\Sigma_\tau^o = 21.2$ (35) and $\beta_f \approx 1.1 \times 10^{-3}$ °C^{-1} (see Figure 3). Values of $\mathcal{B}$(36), at this depth, are in the range between 0.34 and 0.0034 corresponding to the range of characteristic fault temperatures between $\theta_* = 17$°C and $\theta_* = 0.17$°C (or fault thickness between $\lambda_o = 1$ cm and $\lambda_o = 1$ m), respectively.

[38] The condition that the initial slip rate be positive (31) can be expressed as a requirement that the dilatancy exceeds a minimum value $\Phi_{\min}$. The value of $\Phi_{\min}$ given by (32) can then be expressed as a function of depth by using (35) and (36) and the depth dependence of β_f (Figure 3). For $\Phi_{\min} < 0$, the slip rate at peak stress (initial slip rate) is positive for any (nonnegative) dilatancy Φ. Because $\mathcal{B}$ and Σ_τ^o increase with depth, so does $\Phi_{\min}$. Consequently, there exists a maximum depth, depending on the characteristic temperature, below which slip weakening is inherently unstable (i.e., initial slip rate is negative) if $\Phi < \Phi_{\min}$. If slip initiates before rather than at peak stress, as assumed here, the initial slope of the slip weakening relation $d\tau_{fl}/d\delta$ must exceed a minimum (positive) value for stable slip at depths below this maximum (see (16)). For $p_* = 5$ MPa and sufficiently low characteristic temperatures (e.g., $\theta_* = 1.7$°C) or, equivalently, for sufficiently wide fault zones ($\lambda_o = 10$ cm), the values of β_f and K_f^{-1} in the entire depth range from 0 to 10 km (Figure 3) are such that the initial slip rate is positive regardless of the fault dilatancy. On the other hand, for large characteristic temperatures (e.g., $\theta_* = 17$°C), or narrow fault zones ($\lambda_o = 1$ cm), slip is inherently unstable for small amounts of dilatancy ($0 < \Phi < \Phi_{\min}$) at all but very shallow depths (less than about 2 km). Thus, the fault thickness (or, more precisely, its product with C) is a crucial parameter for evaluating slip stability (at least in the small dilatancy case): an increase by one order of magnitude (from $\lambda_o = 1$ cm to $\lambda_o = 10$ cm) results in change from initially unstable to initially stable slip at almost all depths down to 10 km for small dilatancy Φ.

5. Limiting Cases

[39] In this section, we consider a number of limiting cases. These accurately describe the response over some portion of the slip history. In addition, they illuminate certain important effects that frictional heating can have on the slip and its stability that will be helpful in understanding more complex cases.

5.1. Slip in the Absence of Strength Weakening and Dilation

5.1.1. Analysis and Stability Considerations

[40] The limiting case of no inelastic strength weakening, $\mathcal{A} = 0$, and no dilation of the slip layer, $\Phi = 0$, will apply

when the amount of sliding exceeds the residual amount of slip δ_r, $\delta > \delta_r$ ($\Delta > 1$). This also corresponds to the dilationless case considered by *Lachenbruch* [1980] but includes fluid and heat transport. In this case, the dimensionless pressure Π and slip Δ are related by $\Pi = \Delta - T$ (22) and (27) and (28) can be reduced to the following two equations in terms of Π and Θ (rather than Δ and Θ, as before)

$$D\dot{\Pi} = -\frac{1}{\epsilon}\Pi + \mathcal{B}\left[\Sigma_\tau - \frac{1}{\epsilon_\chi}\Theta\right] \tag{37}$$

$$D\dot{\Theta} = -\frac{1}{\epsilon}\Sigma_\tau\Pi + \left[\Sigma_\tau - \frac{1}{\epsilon_\chi}\Theta\right] \tag{38}$$

where, according to (25) and (30) with $\mathcal{A} = \Phi = 0$, respectively,

$$\Sigma_\tau = \Sigma_\tau^o - \mu_o\Pi,\ D = 1 - \mathcal{B}\Sigma_\tau \tag{39}$$

Recall that coefficient D also appears in an equation for the slip rate (27), $D\dot{\Delta} = N/\epsilon$, with N given by (29).

[41] Equation (37) shows that as long as $D > 0$ shear heating tends to cause an increase in the pore pressure, which can, however, be offset by fluid diffusion. The increase in the pore pressure causes reduction of the shear resistance, and, since the shear stress must equal the resistance, of the shear stress Σ_τ(39). The reduction in shear stress increases the coefficient D. This simple observation suggests that instability corresponding to the unbounded slip rate ($D = 0$) can only take place when D is negative at some moment of slip history.

[42] This conjecture is readily verified by noting that (37) and (38) have the steady slip solution, $\Pi^{ss} = 0$, $\Theta^{ss} = \epsilon_\chi\Sigma_\tau^o$, and $\dot{\Delta}^{ss} = 1$. This corresponds to thermal conduction that exactly compensates for shear heating to maintain the temperature increase and no change in pore pressure. Solutions of (37) and (38) linearized about this steady state have the form of constants multiplied by $\exp(aT/\epsilon)$, where a satisfies a quadratic equation (see Appendix B for more details). For $\epsilon \ll 1$, the solutions for a are $-(\epsilon D_o)^{-1}$ and $-\epsilon_\chi^{-1}$, where $D_o = 1 - \mathcal{B}\Sigma_\tau^o$. Hence if $D_o > 0$, both solutions for a are negative and any small perturbations from the steady state solution decay exponentially to zero. Alternatively, if $D_o < 0$, this linear analysis shows that no steady sliding is possible as any small perturbation from the steady state grows exponentially with time.

[43] The restriction that the initial slip rate be positive ((31) with $\Phi = 0$) requires that $D_o > 0$ if the initial temperature and pressure equal their ambient values, i.e., when $\Pi = \Pi_o = 0$ and $\Theta = \Theta_o = 0$. However, the no weakening, no dilation case may be preceded by an episode during which the temperature and pressure do not equal their ambient values. For $\Pi \neq 0$ and $\Theta \neq 0$, it is possible to have a solution for positive slip rate with $D_o < 0$. The analysis in Appendix B shows, however, that any such solution (not just one near steady state) evolves either to instability in the form of an unbounded slip rate ($\dot{\Delta} \to \infty$) or to arrest ($\dot{\Delta} = 0$). (As will be discussed in more detail in the companion paper (Garagash and Rudnicki, submitted manuscript, 2002), arrest appears to be an anomaly resulting from over simplification of the description of friction.) Interestingly, solutions with $\dot{\Delta} > 0$ and $D_o < 0$ require $\Pi > 0$ and, hence, a pore pressure in excess of ambient. Such a situation could occur following pressure buildup in a thermally and hydraulically sealed, nondilating fault zone [*Blanpied et al.*, 1992], fault compaction [*Sleep and Blanpied*, 1992] or the arrival of a pressure pulse from depth [*Rice*, 1992].

[44] The condition $D_o < 0$ implies that the ambient level of shear stress exceeds the critical value,

$$\Sigma_\tau^o > \mathcal{B}^{-1}\ \text{(slip instability)} \tag{40}$$

or equivalently in the dimensional form

$$\tau_o > \frac{(G/\mu_o)C}{K'\beta'}\frac{\lambda_o}{\ell} \tag{41}$$

Since τ_o and β' (among other parameters) are increasing with depth, the condition (41) suggests decreasing stability with depth. The conclusion just stated requires that ϵ be small and, hence, that drainage from the fault be rapid compared with the imposed deformation rate. As discussed above, this will generally be the case, but, if the fault zone is hydraulically sealed [*Blanpied et al.*, 1992], drainage will not be possible and solutions for large ϵ will be appropriate.

5.1.2. Interpretation in Terms of the Physical Parameters

[45] Consider the interpretation of the slip instability condition (40) or (41) in terms of the physical parameters. As discussed previously, the ambient dimensionless stress Σ_τ^o and its critical value $\mathcal{B}^{-1}$ depend on the depth of the slip. For particular choice of parameters of the fault system corresponding to the characteristic pressure $p_* = 5$ MPa, the depth dependence is prescribed by (35) and (36) where variation of dimensional pore fluid properties with depth are given by the plot on Figure 3. It is easily verified that $\mathcal{B}^{-1}$ (Σ_τ^o) is decreasing (increasing) with depth. For the various values of characteristic temperature $\theta_* = \{1.7°C, 3.3°C, 17°C\}$ (corresponding to the values of fault thickness $\lambda_o = \{10, 5, 1$ cm$\}$) (see section 4), the instability condition (40) is satisfied when depth $d > d^*$ with $d^* \approx \{1.6, 6.2, 10\}$ km. Consequently, slip is stable in depth range 0–10 km (unstable except at shallow depths) for sufficiently low (high) characteristic temperature or, equivalently, for sufficiently wide (narrow) fault zone. Thus, the fault thickness is a crucial parameter in evaluation of slip stability: increase by one order of magnitude (from $\lambda_o = 1$ cm to $\lambda_o = 10$ cm) yields change from unstable to stable behavior (in the context of zero weakening and dilatancy) at almost all depths in the considered range.

[46] It is instructive to estimate physical values of various quantities considered including values of pressure and temperature rise at instability over the corresponding ambient levels. As an example, consider the case $\theta_* = 3.3°C$ ($\lambda_o = 5$ cm) for which the critical depth is $d^* \approx 6.2$ km. The values of relevant dimensionless parameters are as follows: for the stable slip at depth $d = 4$ km, $\{\Sigma_\tau^o, \mathcal{B}^{-1}, 10^3\Theta^{ss}\} = \{11.6, 20.6, 8.7\}$, and, for the unstable slip at depth $d = 8$ km, $\{\Sigma_\tau^o, \mathcal{B}^{-1}, 10^3\Theta^{ss}\} = \{21.2, 14.8, 16\}$. For $d = 8$ km, pressure rise and temperature rise at instability can be computed from the solutions of Appendix B and scaling (21) as $p - p_o \approx 53.5$ MPa and $\theta - \theta_o \approx 635°C$. These large values suggest that pore fluid properties can be altered significantly from their ambient values in the course of the slip leading to the

instability. These alterations (presently not accounted for in the model) can affect the slip evolution toward the instability (or even the instability itself) and, therefore, should be taken into consideration in the further work.

5.2. Fully Drained Slip ($\epsilon = 0$)

[47] Because $\epsilon \ll 1$ (34) most of the time the slip is so slow compared to the pore fluid diffusion rate that the pore pressure does not change from its ambient value. In the limit, $\epsilon = 0$, (23) indicates that the pore pressure remains constant, $\Pi = 0$ and, according to (22), the solution for the slip Δ is given in implicit form

$$T = T_d(\Delta) = \Delta - \frac{2}{3}\mathcal{A}g(\Delta) \text{ or} \dot{\Delta} = \left(1 - \frac{2}{3}\mathcal{A}g'(\Delta)\right)^{-1} \quad (42)$$

Multiplication of (24) by $\dot{\Delta}^{-1}$ from (42) yields an equation for temperature Θ variation with the slip Δ

$$\frac{d\Theta}{d\Delta} = \Sigma_\tau - \frac{1}{\epsilon_\chi}\Theta\left(1 - \frac{2}{3}\mathcal{A}g'(\Delta)\right) \quad (43)$$

According to (25) and (42), Σ_τ is a function of Δ only, $\Sigma_\tau = \Sigma_\tau^o - \mu_o \frac{2}{3}\mathcal{A}g(\Delta)$. Thus, the solution of (43) with the initial condition $\Theta(0) = 0$ is

$$\Theta = \Theta_d(\Delta) = \int_0^\Delta \Sigma_\tau(u) \exp\left[-\frac{T_d(\Delta) - T_d(u)}{\epsilon_\chi}\right] du \quad (44)$$

where $T_d(\Delta)$ in the exponent is time as a function of the slip in the drained solution (42). Note that when $\epsilon_\chi \to 0$ (corresponding to the slip time much larger than the temperature diffusion time, $t_s \gg t_\chi$, see (26)), and the slip rate is finite, $T_d'(\Delta) > 0$, (44) yields zero temperature alteration, $\Theta = 0$, i.e., temperature is equal to its ambient value at all times during the slip.

[48] For $\mathcal{A} < 1$, with g given in Appendix A1 the slip and the slip rate in the drained solution (42) remain bounded for all times. For $\mathcal{A} \geq 1$, we observe, following the study of *Rudnicki and Chen* [1988], that the drained solution (42), (44) leads to an infinite slip rate at $T = T_*$, $\Delta = \Delta_*$, where T_* and Δ_* are functions of $\mathcal{A}$ defined in Appendix A ((A2)–(A3)). The drained solution for the dimensionless slip time T(42) (Figure 4a) and dimensionless temperature rise Θ (44) (Figure 4b) are shown in Figure 4 versus the dimensionless slip Δ for a pair of values of the weakening parameter $\mathcal{A} = \{8/9, 9/8\}$ and $\Sigma_\tau = 10$, $\mu_o = 0.6$, and $\epsilon_\chi = 0.01$. As was discussed above, Figure 4 shows that drained solution is stable for $\mathcal{A} = 8/9 < 1$ and it breaks down at $T = T_* \backsimeq 0.14$ and $\Delta = \Delta_* \backsimeq 0.33$ for $\mathcal{A} = 9/8 > 1$. Although the entire relation (42) for $\mathcal{A} = 9/8$ is shown on Figure 4, only those portions of the plot where the time T is monotonically increasing (solid line) are physically meaningful. Figure 4 also shows that the temperature initially rises as the slip rate increases, reaches a maximum, and decreases to a constant asymptotic value corresponding to the steady slip. For a characteristic temperature θ_* in the range between 17°C ($\lambda_o = 1$ cm) and 0.17°C ($\lambda_o = 1$ m), the maximum $\Theta \approx 0.8$ in the drained solution for $\mathcal{A} = 8/9$ corresponds to the maximum temperature rise $\theta - \theta_o = \theta_* \Theta$ in the range 13.2–0.132°C, respectively. For a representative geothermal gradient of 20–25°C km^{-1}, the estimated temperature rise due to the shear heating is small compared to ambient value θ_o at all but shallow depths. This result supports the neglect of the effect of the slip-induced temperature alterations on the pore fluid properties (K_f and β_f) (see section 4).

[49] The slip rate singularity for $\mathcal{A} \geq 1$ does not, however, necessarily lead to slip instability if conditions are not completely drained. For rapid, but finite drainage, the assumption that $\epsilon\dot{\Delta} \ll 1$ is a good one for most of the slip history but breaks down when $\dot{\Delta}$ becomes comparable to ϵ^{-1} as $T \to T_*$ in (42). Consequently, it is necessary to consider the full equations to account for high slip rates. Analysis of the stability of accelerating ($\mathcal{A} \geq 1$) slip under conditions of rapid fluid drainage $\epsilon \ll 1$ is given in the companion paper (Garagash and Rudnicki, submitted manuscript, 2002).

5.3. Fully Undrained Adiabatic Slip ($\epsilon = \infty$, $\epsilon_\chi = \infty$)

5.3.1. Solution

[50] As noted in the discussion of the fully drained case, the slip rate may become sufficiently rapid that even though $\epsilon \ll 1$, the product $\epsilon\dot{\Delta}$ is order one. In other words, the slip is occurring on a timescale comparable to that of fluid drainage from the fault. For more rapid slip, there will be insufficient time for drainage and conditions will approach undrained. A similar discussion applies for thermal conduction: for rapid slip, conditions will approach adiabatic. This undrained, adiabatic limit may also be relevant for smaller values of the slip rate if the fault zone is hydraulically sealed and thermally isolated from the surrounding material [*Blanpied et al.*, 1992]. In the limit $\epsilon \to \infty$ and $\epsilon_\chi \to \infty$, (27) and (28) with (29) yield

$$D\dot{\Delta} = 1, \ \dot{\Theta} = \Sigma_\tau \dot{\Delta} \quad (45)$$

where D is the function of T and Δ given by (30), and Σ_τ is given by (25). Because D is a linear function of T through dependence on Σ_τ, the first of (45) can be integrated to provide time T as a function of the slip Δ in undrained solution, $T = T_u(\Delta)$,

$$T_u(\Delta) = \int_0^\Delta \left[\Phi f'(u) + 1 - \frac{2}{3}\mathcal{A}g'(u) - \mathcal{B}\left(\Sigma_\tau^o - \mu_o u\right)\right] e^{-\mu_o \mathcal{B}(\Delta - u)} du \quad (46)$$

The integral in (46) can be carried out explicitly but the result is not recorded here because of its length. The pressure, $\Pi = \Pi_u(\Delta)$, is found from substituting (46) into (22) and the temperature $\Theta = \Theta_u(\Delta)$ from integration of the second equation in (45).

[51] For $\Delta \geq 1$, the effects of frictional weakening and dilatancy saturate and the solution assumes the relatively simple form

$$\begin{aligned} T_u(\Delta) &= \Delta - \frac{\Sigma_\tau^o}{\mu_o} + e^{-\mu_o \mathcal{B}(\Delta - 1)}\left[T_u(1) - \left(1 - \frac{\Sigma_\tau^o}{\mu_o}\right)\right] \\ \Pi_u(\Delta) &= \frac{\Sigma_\tau^o}{\mu_o} - \frac{2}{3}\mathcal{A} - e^{-\mu_o \mathcal{B}(\Delta - 1)}\left[T_u(1) - \left(1 - \frac{\Sigma_\tau^o}{\mu_o}\right)\right] \\ \Theta_u(\Delta) &= \Theta_u(1) + \frac{1}{\mathcal{B}}\left[1 - e^{-\mu_o \mathcal{B}(\Delta - 1)h}\right]\left[T_u(1) - \left(1 - \frac{\Sigma_\tau^o}{\mu_o}\right)\right] \end{aligned} \quad (47)$$

For large slip Δ (although instability may occur first), the exponential terms in (47) vanish, yielding an asymptotically constant slip rate, $\dot{\Delta} = 1$, constant pressure $\Pi_u(\infty) = \Sigma_\tau^o/\mu_o - (2/3)\mathcal{A}$ and temperature (for $\mathcal{B} > 0$). The residual value of the pressure for $\mathcal{B} > 0$ is equal to the normalized residual

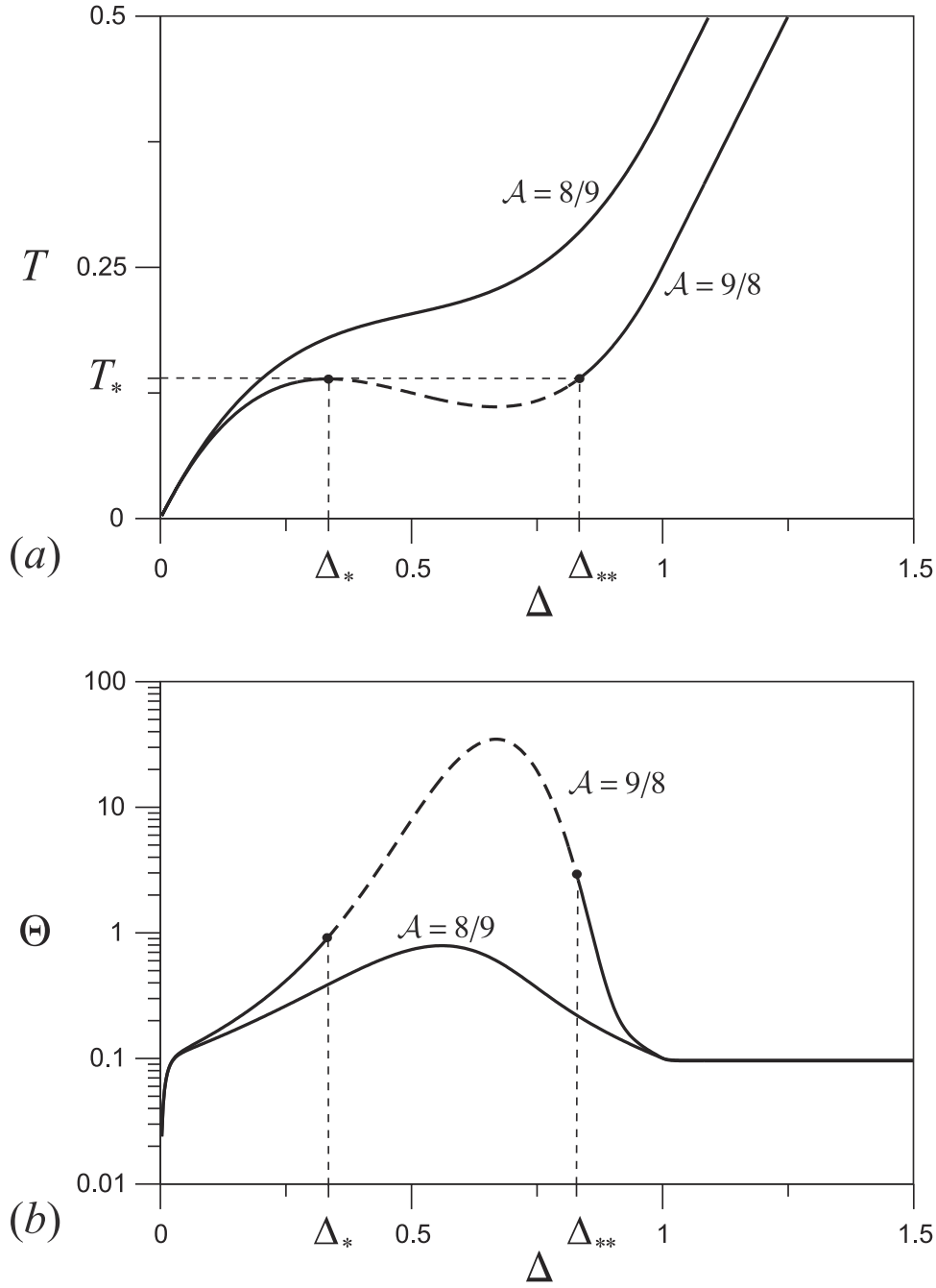

Figure 4. Plots of (a) dimensionless slip time T and (b) dimensionless temperature rise Θ versus dimensionless slip Δ in the drained solution for two values of $A = \{8/9, 9/8\}$ and $\Sigma_\tau^o = 10$, $\mu_o = 0.6$, and $\epsilon_\chi = 0.01$. Drained slip instability occurs for $A = 9/8$ at $\Delta = \Delta_*$.

strength of the fault (18) $\Pi_u(\infty) = \tau_{r'}/(\mu_o p_*)$, and, therefore, is always nonnegative. It corresponds to the maximum pressure attained during undrained adiabatic slip if the pressure decreases upon the slip initiation. (The latter requires $2\Phi > \mathcal{B}\Sigma_\tau^o$). Because the fault is assumed to be adiabatic (no heat loss) and undrained (no fluid loss), it may be surprising that the temperature and pore pressure approach a constant finite value for large slip Δ. This result is, however, explained by noting that the shear stress on the fault asymptotically approaches zero, $\Sigma_\tau = 0$ (see (25) and (47)). Thus, in this limit, the fault is slipping steadily at the far-field rate under zero shear stress. In the thermomechanical uncoupled case, $\mathcal{B} = 0$, the pressure for slip beyond residual is constant and equal to its minimum value, $\Pi_u(\Delta \geq 1) = -\Phi$, while the temperature increases linearly for large Δ rather than approaching a constant value. This minimum value provides the lower bound to the pressure change during undrained slip for the coupled case $\mathcal{B} > 0$.

[52] The features of the undrained adiabatic solution are illustrated in Figure 5. The time T, pressure rise Π and temperature rise Θ are plotted against slip Δ for $\mathcal{A} = 2$, $\Phi = 7$, $\Sigma_\tau^o = 10$ and $\mu_o = 0.6$ and three values of $\mathcal{B} = \{0, 0.075,$

0.1}. The slip rate remains bounded for the lower two values, but becomes infinite for $\mathcal{B} = 0.1$. The pressure Π initially decreases with slip due to the fault dilatancy (Figure 5b) and reaches its minimum value, bounded from below by the value $-\Phi$, when the decreasing rate of dilatancy is balanced by thermal expansion. Thereafter the pressure increases with the slip to reach its positive asymptotic value $\Sigma_\tau^o/\mu_o - (2/3)\mathcal{A}$. The temperature increases monotonically with the slip (Figure 5c). These constant asymptotic values of pressure and temperature for $\mathcal{B} > 0$ are attained only after slip distances of about $10^2\delta_r$. The large slip asymptotic values of the pressure $\Pi \sim 10$ and temperature $\Theta \sim 10^2$ (Figures 5b and 5c) correspond to large dimensional pressure and dimensional temperature rises of about 50 MPa and 330°C (for the choice of $p_* = 5$ MPa and $\theta_* = 3.3$°C). In contrast to the fully drained slip, the alteration of the pore fluid properties at large amounts of undrained adiabatic slip can be significant and should be included in more elaborate modeling.

5.3.2. Stability Considerations and Parametric Dependence

[53] As seen from Figure 5, the undrained slip rate can become unbounded with sufficient shear heating. However, even when slip rate remains bounded instability may occur by either cavitation or hydraulic fracture. The former is caused by dilatant pore pressure reduction at early stages of the slip and the latter by pore pressure increase (for $\mathcal{B} > 0$) due to the shear heating in the later stages of the slip (see Figure 5b).

5.3.3. Instability Due to Cavitation

[54] As noted by *Rudnicki and Chen* [1988], if pore pressure drops below the cavitation limit, instability occurs because of a severe reduction in pore fluid bulk modulus. For the temperature range characteristic of the shallow crust, the cavitation limit can be approximated by zero. Thus, the minimum value of the pore pressure is bounded from below by its value for zero thermomechanical coupling $\mathcal{B} = 0$,

$$p_{\inf} = p_o - \Phi p_* = p_o - \phi_r^p K' \tag{48}$$

Therefore, a sufficient condition for the cavitational instability is that $p_{\inf} \leq 0$ (this condition is also necessary for no thermomechanical coupling $\mathcal{B} = 0$). For $\Phi = 7$ considered in Figure 5, the characteristic value of pressure $p_* = 5$ MPa and hydrostatic pore pressure p_o gradient of 10 MPa km^{-1}, this condition is met for depths shallower than 3.5 km.

5.3.4. Instability Due to Hydrofracture

[55] The dimensional form of the maximum value of the pressure attained for large slip and $\mathcal{B} > 0$ is

$$p_{\max} = p_o + \left(\frac{\Sigma_\tau^o}{\mu_o} - \frac{2}{3}\mathcal{A}\right)p_* = p_o + \tau_r/\mu_o \tag{49}$$

If this value exceeds the least compressive stress, $\sigma_{\min}$, then hydrofracture occurs. Although this condition is simple to evaluate, it is necessary to know the stress state and fault orientation at the particular site.

5.3.5. Instability With Unbounded Slip Rate

[56] Slip instability with unbounded slip rate $\dot{\Delta} = \infty$ takes place whenever $T_u'(\Delta) = D(T_u(\Delta), \Delta) = 0$ (45). Thus, undrained slip is stable if the latter equation has no real positive roots. For $\Delta > 1$, (47) indicates that $T_u'(\Delta) > 0$ if $T_u'(1) > 0$. Thus, slip instability ($T_u'(\Delta) = 0$) cannot occur for $\Delta > 1$. For $\Delta \leq 1$, the roots of $T_u'(\Delta) = 0$, which give the

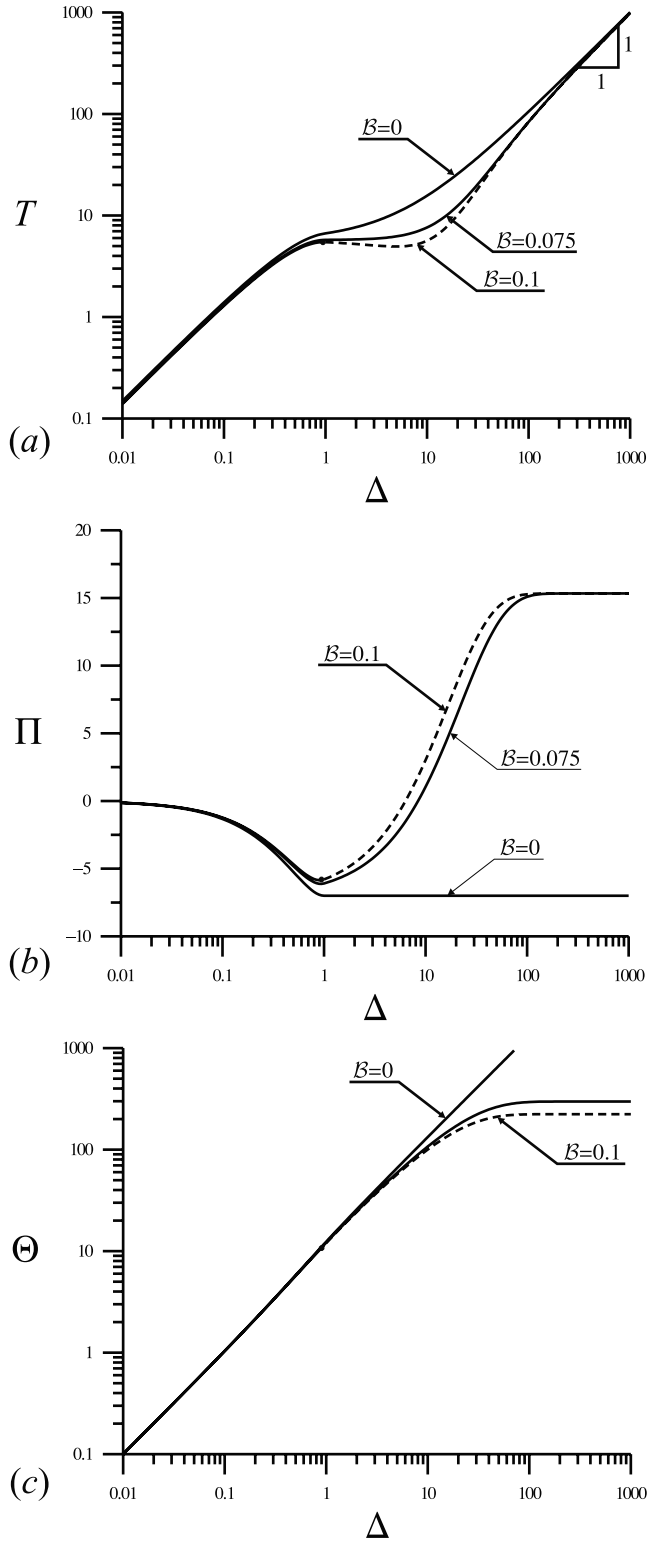

Figure 5. Plots of (a) time T, (b) pressure Π, and (c) temperature Θ versus slip Δ for various $B = \{0, 0.075, 0.1\}$ and $A = 2$, $\Phi = 7$, $\Sigma_\tau^o = 10$, $\mu_o = 0.6$ in log–log scale (T and Θ versus Δ) and semilog scale (Π versus Δ). (Physically meaningless parts of solution after the instability are shown by the dashed line.)

boundaries of the domain of stable slip, can be determined explicitly (see Appendix C for details). Figure 6 plots the slip stability domain in the parameter plane of dilatancy (Φ) against slip weakening ($\mathcal{A}$) for four values of thermomechanical coupling parameter $\mathcal{B} = \{0, 0.05, 0.075, 0.1\}$.

[57] When slip is uncoupled from temperature changes ($\mathcal{B} = 0$), the stability domain lies above the dashed line given by $\Phi = 2(\mathcal{A} - \sqrt{\mathcal{A}})$. For $\mathcal{A} < 1$ slip is stable in the fully drained case and, hence, is also stable in the undrained case for any amount of dilatancy. For a fixed value of the weakening $\mathcal{A} > 1$, slip is unstable in the fully drained case but can be stabilized by sufficiently large dilatancy. Similarly, for a fixed value of the dilatancy Φ, sufficiently strong slip weakening will cause instability. This result differs from that of *Rudnicki and Chen* [1988] who found that undrained response was always stabilized by even a very small amount of dilatancy as long as the pressure drop was not sufficient to cause significant reduction in the pore fluid bulk modulus K_f. This feature of their analysis is due to the neglect of the initial thickness of the fault zone (assumed to be infinitesimally thin) and the normal elastic stiffness of the fault zone.

[58] Figure 6 demonstrates that the region of stable slip decreases monotonically with the thermomechanical coupling $\mathcal{B}$. The stability domain shrinks to a point as $\mathcal{B}$ approaches the critical value $\mathcal{B}_\infty = 1/(\Sigma_\tau^o - \mu_o)$, given by the solution of the instability condition $D = 0$ for $\mathcal{A} = 0$, $\Phi = \Phi_{\min}$ and $\Delta = 1$ (the value of slip at instability for this case). The limiting point is $(0, \Phi_\infty)$ where Φ_∞ is the minimum dilatancy value for slip initiation $\Phi_{\min}(32)$ evaluated at $\mathcal{B} = \mathcal{B}_\infty$. Consequently, undrained slip is unstable for any amount of dilatancy, $\Phi \geq 0$, and slip weakening, $\mathcal{A} \geq 0$, if

$$\mathcal{B} \geq \mathcal{B}_\infty \equiv \frac{1}{\Sigma_\tau^o - \mu_o} \tag{50}$$

or in the dimensional form

$$\tau_o \geq G\frac{\delta_r}{\ell} + \frac{(G/\mu_o)C}{K'\beta'}\frac{\lambda_o}{\ell} \tag{51}$$

For the choice of parameters of Figure 6, $\Sigma_\tau^o = 10$, $\mu_o = 0.6$, the critical normalized thermal expansion is $\mathcal{B}_\infty \approx 0.1064$. For $p_* = 5.0$ MPa, $K' = 2.0$ GPa and $\theta_* = 1.7°C$, the corresponding value of $\beta' = 1.6 \times 10^4\ °C^{-1}$. For $\beta' = \phi_0\beta_f$ and $\phi_0 = 0.05$, the value of β_f is 3.1×10^{-3}. This is about a factor of 2 larger than the largest values shown in Figure 3. This suggests this condition will not be met ordinarily but may be possible for locally or temporarily high values of β', etc.

[59] As $\mathcal{B}$ is increased from zero, the minimum value of Φ for stability (at a fixed value of $\mathcal{A}$) increases expanding the unstable domain. This effect is anticipated because the increase in pressure due to heating competes with the decrease due to dilatancy. Less obvious is the emergence of an upper boundary to the stable region (in terms of Φ) as soon as $\mathcal{B} > 0$. In other words, for a fixed value of weakening $\mathcal{A}$, an increase in dilatancy does not continue to stabilize slip: there is a maximum value of Φ for which slip is stable. Furthermore, if $\mathcal{A}$ is large enough, slip becomes unstable for any $\Phi \geq 0$. The emergence of the upper stability boundary in terms of Φ can be explained along the following lines. The pore pressure drop due to fault dilatancy increases the effective confining stress and, consequently, the frictional resistance of the fault. This is a stabilizing effect on the slip. On the other hand, the same increase of shear stress due to dilation facilitates shear heating (proportional to Σ_τ). Shear heating tends to increase the pressure and, therefore, to destabilize the slip. These two competing effects of dilatancy cause the appearance of the upper Φ stable limit. Indeed, dilatancy counteracts the destabilizing effect of fault frictional strength weakening (quantified by $\mathcal{A}$) before both effects saturate ($\Delta < 1$). Because both effects vanish when slip Δ approaches unity, the increase in Σ_τ due to past fault dilation can be sufficient for shear heating to destabilize the slip.

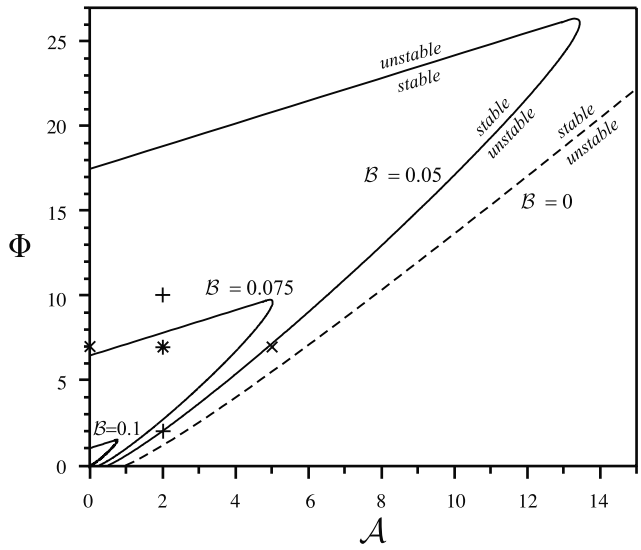

Figure 6. Slip stability domain the parameter plane of dilatancy (Φ) against slip weakening (A) for four values of thermomechanical coupling parameter $B = \{0, 0.05, 0.075, 0.1\}$ and $\Sigma_\tau^o = 10$, $\mu_o = 0.6$. The stability domain lies above the dashed line for the case $B = 0$. For $B > 0$, the stable domain is finite and bounded by the curves shown. The stability domain shrinks to the point ($A = 0$, $\Phi_\infty \approx 0.032$) as $B \to B_\infty \approx 0.1064$.

[60] Similarly to the stability dependence on the dilatancy Φ discussed above, dependence of the slip stability on the fault weakening $\mathcal{A}$ is also nonmonotonic. That is for fixed nonzero values of thermomechanical coupling $\mathcal{B}$ and dilatancy Φ (larger than the value given by the intersection of the upper branch of the stability boundary for constant $\mathcal{B}$ with $\mathcal{A} = 0$ axis in the ($\mathcal{A}$, Φ) plane on Figure 6), the slip is unstable for small enough as well as large enough values of weakening $\mathcal{A}$. The latter effect is easily anticipated, as larger weakening tends to destabilize the fault. The former effect corresponding to the existence of the lower boundary to the stable region in terms of $\mathcal{A}$ is less obvious, but can be explained along the same lines as the dilatancy effect in the preceding paragraph. Indeed, a smaller amount of fault weakening allows the fault to sustain its frictional resistance in the course of the slip. This is a stabilizing effect. On the other hand, higher shear stress sustained in the course of the slip (as compared with situations with larger fault weakening) causes higher levels of shear heating. Higher shear heating tends to increase the pore pressure and, therefore, destabilize the slip. These two

competing effects of the weakening cause the appearance of the positive lower $\mathcal{A}$ stable limit.

5.3.6. Illustrative Examples

[61] Different effects of increasing dilatancy or increasing weakening on slip instability with unbounded slip rate, as discussed above, are illustrated in Figure 7. Figures 7a–7c show the undrained solution for three values of dilatancy $\Phi = \{2, 7, 10\}$ and a fixed value of weakening $\mathcal{A} = 2$ (see the points indicated by straight crosses on Figure 6); and Figures 7a′–7c′ show the undrained solution for a fixed value of dilatancy $\Phi = 7$ and three values of weakening $\mathcal{A} = \{0, 2, 5\}$ (see the points indicated by inclined crosses on Figure 6). The other parameters are fixed for both sets in Figure 7: thermal coupling $\mathcal{B} = 0.075$, friction coefficient $\mu_o = 0.6$, and initial shear stress $\Sigma_\tau^o = 10$. The solution with $(\mathcal{A}, \Phi) = (2, 7)$ is common to the both sets and falls within the stability region for $\mathcal{B} = 0.075$ (Figure 6).

[62] Consider first the solutions for various dilatancy values at fixed weakening $\mathcal{A} = 2$ (Figures 7a–7c). Instability for $\Phi = 2$ occurs well inside the slip interval $0 \le \Delta \le 1$ and signifies that this level of dilatancy is not sufficient to overcome the destabilizing effect of fault frictional weakening. Indeed, Figure 7b shows that the dilatant pressure drop for the unstable case $\Phi = 2$ is smaller than that for the stable slip with the higher value of dilatancy $\Phi = 7$. On the other hand, the relatively small temperature increase Θ at slip instability for $\Phi = 2$ (Figure 7c) indicates that frictional weakening rather than shear heating is the primary cause of instability for small values of dilation and $\mathcal{A} = 2$. Slip is also unstable for $\Phi = 10$, but now the instability takes place near $\Delta = 1$ (Figure 7a). This indicates that dilatancy is high enough to counteract the effect of fault weakening during nearly all of the interval $0 \le \Delta \le 1$. However, dilatancy also increases the shear resistance and, consequently, the shear heating, high enough for instability to take place as dilatancy vanishes (Δ approaches 1). Instability for the case $\Phi = 10$ occurs at a temperature Θ significantly higher than in the small dilation case $\Phi = 2$ (Figure 7c), and slightly past the minimum value of pressure Π (Figure 7b, corresponding to the onset of fault pore fluid repressurizing, $\dot{\Pi} \ge 0$, after dilatant pressure drop, $\dot{\Pi} < 0$).

[63] Similar discussion pertains to the solutions for various weakening at fixed dilatancy $\Phi = 7$ (Figures 7a′–7c′). Notably, instability for larger value of weakening $\mathcal{A} = 5$ occurs well inside the slip interval $0 \le \Delta \le 1$ (Figure 7a′), and indicates that frictional weakening rather than shear heating is the primary instability mechanism. On the other hand, instability for smaller value $\mathcal{A} = 0$ takes place near $\Delta = 1$ (Figure 7a′), which indicates that instability is caused by the shear heating at the stages of the slip when dilatancy effect vanishes (as $\Delta \to 1$).

6. Concluding Discussion

[64] This paper has studied the effect of shear heating on slip stability for three sets of limiting conditions: (1) no dilation and no frictional weakening, (2) fully drained conditions implying that the fault is hydraulically equilibrated with the surrounding rock at all times, and (3) fully undrained adiabatic conditions.

[65] The first case isolates the effect of shear heating. Frictional heating causes the pore fluid in the gouge zone to expand and, when this expansion is not alleviated by flow, the pore pressure increases. This increase decreases the effective normal stress and, consequently, the resistance to slip. Reduction of the resistance to slip is destabilizing, but, the reduction also reduces the level of shear stress (equal to the resistance by equilibrium) that drives frictional heating. Consequently, we have shown that, if the thermal pressurization is not too large, then there is a solution for steady slip at the tectonic rate with no pore pressure change and shear heating that is exactly compensated by heat flow from the fault zone. This solution, however, becomes unstable with respect to an arbitrary slip perturbation when the initial value of the normalized shear stress Σ_τ^o exceeds the normalized ratio of the fluid compressibility and thermal expansivity $\mathcal{B}^{-1}$. Since the ambient shear stress and pore fluid thermal expansion increase with depth (and other parameters may also depend on depth), the occurrence of this instability depends on the depth.

[66] Because the rate of imposed tectonic straining is so much slower than the rate of fluid exchange between the fault and the surroundings, the fully drained case is a good approximation for most of the slip history. This approximation breaks down if the slip weakening and shear heating are sufficient to cause slip instability in the fully drained case. In order to analyze the approach to instability and determine whether it does, in fact, occur, it is necessary to relax the assumption that the response is fully drained although we can still exploit the smallness of the tectonic strain rate by comparison with the rates of fluid and heat transfer. The analysis of this case is presented in the companion paper.

[67] Fully undrained and adiabatic conditions apply for a fault zone that is hydraulically and thermally isolated from the surrounding rock mass. They will also apply if the slip rate approaches instability and becomes more rapid than the rates of fluid and heat exchange. In the absence of shear heating, *Rudnicki and Chen* [1988] found that stability could be prevented in the undrained case by an arbitrarily small amount of dilatancy, at least if the ambient pressure was sufficient to prevent cavitation. Because we include a finite initial thickness to the fault zone (absent in the analysis of *Rudnicki and Chen* [1988]), we find that a finite magnitude of dilatancy, related to the amount of slip weakening, is necessary to prevent instability. In the absence of shear heating, increased dilatancy tends to inhibit instability and more rapid decrease of stress with slip (slip weakening) tends to promote instability. To a certain extent, this is also the case when shear heating is included. These effects have been discussed previously by *Lachenbruch* [1980] and *Mase and Smith* [1987], although, as noted earlier, these analyses do not include an explicit model of instability. The analysis here shows, however, that with shear heating, increased dilatancy can promote instability and increased slip weakening can inhibit instability. The identification of these effects is significant because they are opposite to those usually associated with dilatancy and slip weakening. They are related to the dependence of shear heating on the absolute stress level (not just its change.) In short, the increase of effective compressive stress caused by dilatancy increases the rate of shear heating and the decrease of shear stress caused by slip weakening decreases the rate of shear heating. Although it is difficult to state precisely appropriate values for material and transport properties, these effects appear for even small

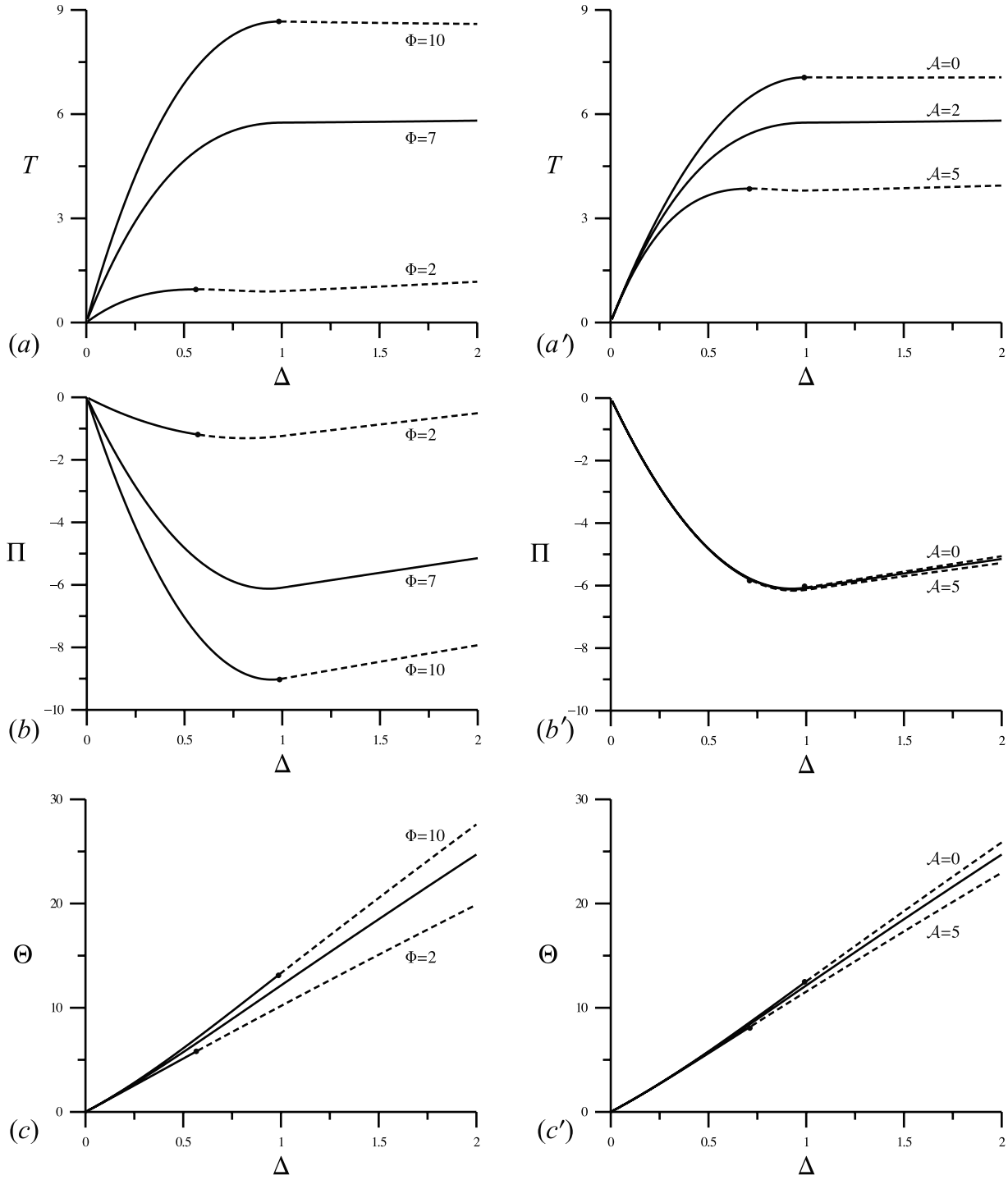

Figure 7. (a)–(c): Dependence of the slip stability in undrained regime on the fault dilatancy: (a) time T, (b) pressure rise Π, and (c) temperature rise Θ versus slip Δ for various $\Phi = \{2, 7, 10\}$ and fixed $A = 2$ (see points marked by the straight crosses on the (A, Φ) plane, Figure 6). (a′)–(c′): Dependence of the slip stability in undrained regime on the fault weakening: (a′) T, (b′) Π, and (c′) Θ versus Δ for fixed $\Phi = 7$ and various $A = \{0, 2, 5\}$ (see points marked by the inclined crosses on Figure 6). Fixed values of the other parameters are $B = 0.075$, $\Sigma_\tau^o = 10$, and $\mu_o = 0.6$. Physically meaningless parts of the slip after an instability (marked by a dot) are shown in dashed lines.

amounts of shear heating and occur in a range of other parameters that is reasonable for faults at depths up to 10 km.

[68] Because shear heating depends on the absolute stress level, it is inherently depth dependent. In addition, the occurrence of instability is related not only to strength parameters (e.g., peak stress and slip weakening) but also to the thermal and hydraulic properties of the pore fluid. Since the latter are also depth dependent, the depth variation

of slip instability (earthquakes) that has been attributed to the depthwise variation of strength [*Sibson*, 1982, 1983] or rate and state friction parameters [*Tse and Rice*, 1986], may also depend significantly on the depth variation of thermal and hydraulic properties.

7. Selected Nomenclature

G	Elastic modulus of the crustal rock
C	Heat capacity of the fault gouge
K'	Effective bulk modulus of the gouge (6)
f	Function specifying inelastic dilation of the fault zone with the slip
g	Function specifying frictional stress decrease with the slip
ℓ	Half thickness of the crustal block
$p - p_o$ (Π)[1]	Pore pressure variation in the fault zone
$\theta - \theta_o$ (Θ)	Temperature variation in the fault zone
p_*, θ_*	Characteristic pore pressure and temperature
t (T)	Time
t_s, t_κ, t_χ	Characteristic timescales of slip, pore fluid diffusion, and thermal diffusion
δ (Δ)	Fault slip
δ_r	Residual slip distance
$\dot{\gamma}_\ell$	Tectonic shear strain rate
ϵ, ϵ_χ	Dimensionless fluid and heat exchange parameters
λ, λ_o	Current and initial half thickness of the fault zone
μ_o	Friction coefficient
τ (Σ_τ)	Shear stress on the fault
τ_o ($\Sigma_{\tau o}$)	Initial shear stress on the fault
$\tau_o - \tau_r$ ($\mathcal{A}$)	Frictional stress drop (slip weakening)
β' ($\mathcal{B}$)	Thermal expansion of pore fluid (thermomechanical coupling)
ϕ_r^p (Φ)	Measure of fault inelastic dilation

Appendix A: Form of Functions *g* and *f*

[69] The particular forms of the functions g and f, characterizing fault weakening behavior and fault dilation, respectively, are taken after the study of *Rudnicki and Chen* [1988] as

$$f(\Delta) = 2\Delta - \Delta^2, \quad g(\Delta) = -2\Delta^3 + 3\Delta^2 \quad \text{for} \quad 0 \le \Delta \le 1$$
$$f(\Delta) = g(\Delta) = 1 \text{ for } \Delta > 1 \tag{A1}$$

This choice is obviously consistent with modeled fault weakening and dilation (see Figure 2).

[70] Critical values of time T_* and slip Δ_*, Δ_{**} appearing in the fully drained solution with $\mathcal{A} > 1$ (see section 5.2 and Figure 4) for the choice of functions f and g given by (A1) can be expressed as follows

$$T_* = \frac{1}{2}\left[1 - \frac{2}{3}\mathcal{A} + \frac{2}{3}\mathcal{A}\left(1 - \frac{1}{\mathcal{A}}\right)^{3/2}\right] \tag{A2}$$

$$\Delta_* = \frac{1}{2}\left[1 - \left(1 - \frac{1}{\mathcal{A}}\right)^{1/2}\right], \quad \Delta_{**} = \begin{cases} \Delta_{**}^{(1)}, \text{ for } 1 < \mathcal{A} \le \frac{4}{3} \\ \Delta_{**}^{(2)}, \text{ for } \mathcal{A} > \frac{4}{3} \end{cases} \tag{A3}$$

with

$$\Delta_{**}^{(1)} = \frac{1}{2} + \left(1 - \frac{1}{\mathcal{A}}\right)^{1/2}, \ \Delta_{**}^{(2)} = T_* + \frac{2}{3}\mathcal{A} \tag{A4}$$

Note that Δ_{**} is a continuous function of $\mathcal{A}$(A3) as $\Delta_{**}^{(1)} = \Delta_{**}^{(2)} = 1$ at $\mathcal{A} = 4/3$ (A4).

Appendix B: Solutions Near and Away From the Steady State Slip in the Absence of Dilatancy and Frictional Weakening

B1. Solution Near the Steady State

[71] Equations (37) and (38) suggest the existence of a steady slip solution, $\Pi = \dot{\Theta} = 0$ and $\Delta = 1{:}\Pi^{ss} = 0$ and $\Theta^{ss} = \epsilon_\chi \Sigma_\tau^o$. The solution of the equations linearized near steady state has the form

$$\{\Pi, \dot{\Theta}\} = C_1 e^{a_1 T/\epsilon}\mathbf{e}_1 + C_2 e^{a_2 T/\epsilon}\mathbf{e}_2 \tag{B1}$$

where $C_{1,2}$ are arbitrary constants and $a_{1,2}$ and $\mathbf{e}_{1,2}$ are eigenvalues and corresponding eigenvectors, respectively. Under the condition $\epsilon < 1$, the eigenvalues and eigenvectors are

$$a_1 \simeq -(\epsilon D_o)^{-1}, \quad \mathbf{e}_1 \simeq \{1/\Sigma_\tau^o, 1\}$$
$$a_2 \simeq -\epsilon_\chi^{-1}, \qquad \mathbf{e}_2 \simeq \{0, 1\} \tag{B2}$$

If $D_o > 0$, both eigenvalues are negative, $a_{1,2} < 0$, in the phase plane (Π, Θ) and the steady state is a *stable nodal* point. If $D_o < 0$, the eigenvalues are of different sign, $a_1 > 0$, $a_2 < 0$, and the steady state is a *saddle* point with the unstable direction given by $\mathbf{e}_1$. Thus, in the former case the steady state solution is stable with respect to small perturbations (i.e., solution trajectories in its vicinity converge), whereas in the latter case the steady state is unstable with respect to small perturbations (solution trajectories are repulsed from it via unstable eigendirection $\mathbf{e}_1$). Solution trajectories near the steady state on the phase plane (Π, Θ) are shown qualitatively on Figures B1a, B1a′, B1b, and B1b′ in stable ($D_o > 0$) and unstable ($D_o < 0$) cases, respectively. For $\epsilon \ll 1$, $a_1 \gg a_2$ and, consequently, in the normal ("outer") scaling for Π (Figures B1a and B1b) it appears that there is almost no evolution in eigendirection $\mathbf{e}_2$ (coinciding with Θ axis). Analysis of the solution away from the steady state is in order.

B2. Solution Away From the Steady State

[72] When $\epsilon \ll 1$, terms of order ϵ can be neglected in (37) and (38) whenever $\Pi = O(1)$, i.e., away from the steady state zero value, yielding

$$d\Theta = \Sigma_\tau d\Pi, \ D\dot{\Pi} = -\Pi \tag{B3}$$

[1] Parenthesis (·) indicates corresponding dimensionless quantity.

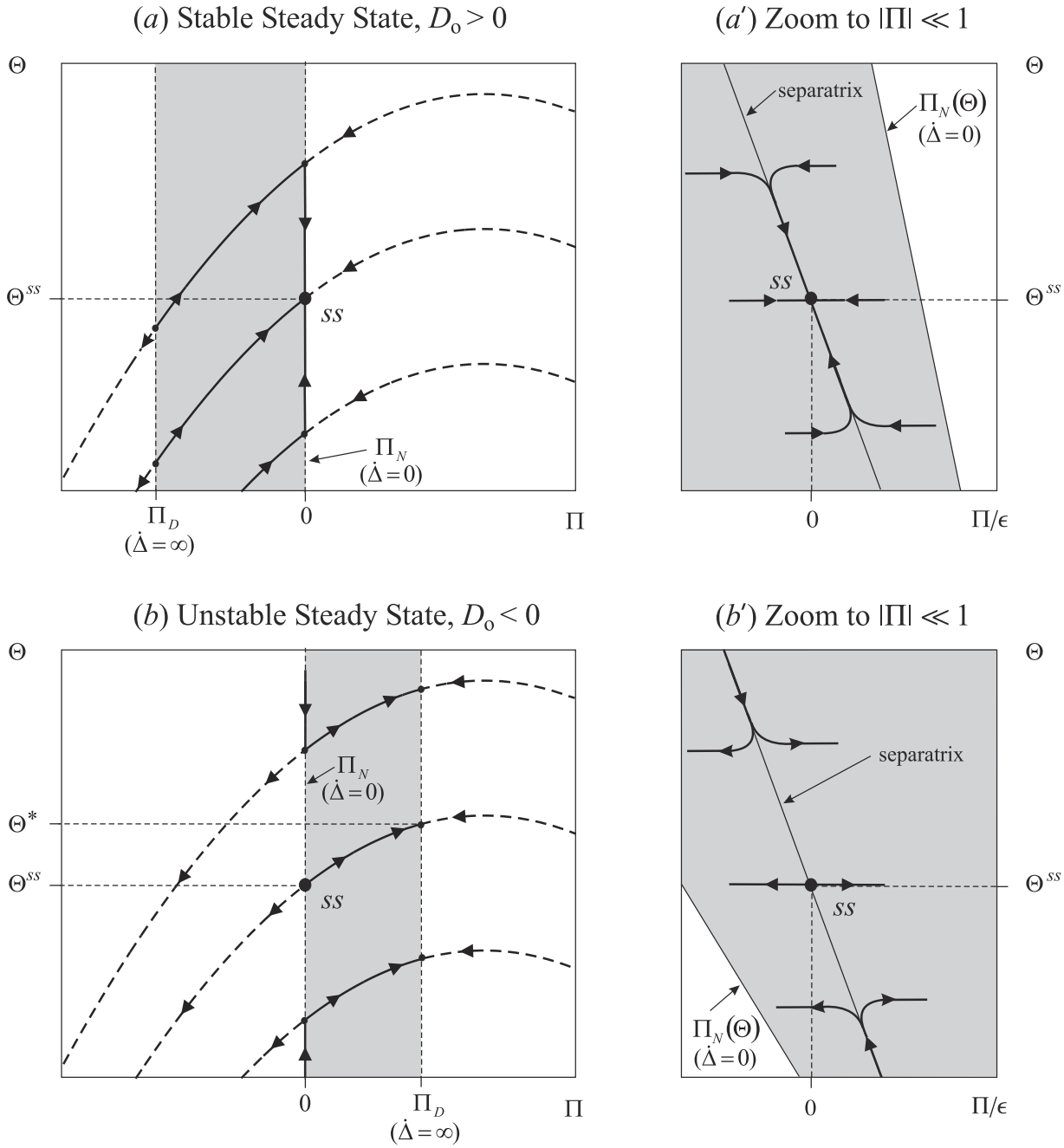

Figure B1. Qualitative sketch of slip solution trajectories in the pressure–temperature plane (Π, Θ) in the absence of fault weakening and dilation $A = \Phi = 0$ and for $\epsilon \ll 1$: (a) and (a′) stable steady state $\Pi = 0$, $\Theta = \Theta_{ss}$ ($D_o > 0$) and (b) and (b′) unstable steady state ($D_o < 0$). Subfigures labeled with prime correspond to the pressure rescaling with ϵ, $\Pi \rightarrow \Pi/\epsilon$, and show details of the solution trajectories in the vicinity of the steady state. Domain of positive slip rate $\dot{\Delta} > 0$ in the (Π, Θ) plane (shown by the shade of gray) is bounded by lines $\Pi = \Pi_D$ and $\Pi = \Pi_N(\Theta)$, which correspond to the unbounded and zero slip rate, respectively. Arrows indicate evolution in time and nonphysical parts of solution trajectories corresponding to negative slip rate are shown by dashed lines.

Upon integration with initial conditions: $\Pi_{|T=To} = \Pi_o$, $\Theta_{|T=To} = \Theta_o$, system (B3) yields the relation between the temperature and the pressure on the fault

$$\Theta - \Theta_1 = \Sigma_\tau^o \Pi - \mu_o \frac{\Pi^2}{2} \tag{B4}$$

and the evolution in time in the implicit form

$$D_o \ln\left|\frac{\Pi}{\Pi_o}\right| + \mu_o \mathcal{B}\,(\Pi - \Pi_o) = -\frac{T - T_o}{\epsilon} \tag{B5}$$

where $\Theta_1 = \Theta_o - (\Sigma_\tau^o \Pi_o - \mu_o \Pi_o^2/2)$ is a value of Θ at which the solution trajectory in the phase plane (Π, Θ) would intersect $\Pi = 0$ (recall that solution (B4) is not valid for $|\Pi| \ll 1$).

[73] According to (B4), solution trajectories in the phase plane are simply parabolas shifted along Θ axis (Figures B1a and B1b). Even though solution (B4) and (B5) is not valid in the vicinity of $\Pi = 0$, it still possesses correct behavior if extended to this vicinity, such that, according to (B5), it takes infinite time to approach ($D_o > 0$) or get away from ($D_o < 0$) the stable separatrix $\Pi \backsimeq 0$. Deviation of the solution from (B4) and (B5) can be seen only in the close vicinity of $\Pi = 0$ (see Figures B1a′ and B1b′).

B3. Slip Stability in the No-Dilatancy, No-Weakening Case

[74] Based on the analysis of preceding paragraphs, Figure B1 shows a qualitative sketch of solution trajectories of (37) and (38) in the pressure–temperature plane (Π, Θ) for $\epsilon \ll 1$: (a)–(a′) stable steady state case $D_o > 0$ and (b)–(b′) unstable steady state case $D_o < 0$ (arrows indicate evolution in time). (Subfigures labeled with a prime correspond to the pressure rescaling with ϵ, $\Pi \to \Pi/\epsilon$, which shows solution details in the immediate vicinity of the steady state for $\epsilon \ll 1$). The domain of positive slip rate $\dot{\Delta} > 0$ in the (Π, Θ) plane (shown by the shade of gray in Figure B1) corresponds to $N/D > 0$ in (27), which in terms of the pressure is

$$\Pi_D \lessgtr \Pi \lessgtr \Pi_N(\Theta) \text{ with } \Pi_D = -\frac{1 - \mathcal{B}\Sigma_\tau^o}{\mathcal{B}\mu_o}, \Pi_N(\Theta) = \epsilon\left(1 - \frac{\mathcal{B}\Theta}{\epsilon_\chi}\right) \tag{B6}$$

The above critical values of pressure correspond to the bounds of the domain of positive slip rate with $\dot{\Delta} = \infty$ at $\Pi = \Pi_D$ and $\dot{\Delta} = 0$ at $\Pi = \Pi_N(\Theta)$ (a small value of order ϵ) (B6). Nonphysical parts of solution trajectories corresponding to negative slip rate (outside of the shaded domain) are shown by dashed lines. Figure B1a shows that slip evolves toward the steady state solution for any initial (perturbed from the steady state) state characterized by positive slip rate (i.e., characterized by initial values of pressure and temperature corresponding to a point in the shaded domain). Due to the rapid drainage, $\epsilon \ll 1$, evolution of slip for $D_o > 0$ (Figure B1a) from an initially perturbed state corresponding to $\Pi = O(1)$ can be approximated, first, by relaxation of the pressure to $O(\epsilon)$ values accompanied by the build up of temperature (following the approximate solution away from the steady state (B4) and (B5)), and, second, by relaxation of temperature toward the steady state value Θ_{ss} accompanied by small ($O(\epsilon)$) changes in pressure. Details of this second part of the slip evolution (in the vicinity of the $\Pi = 0$ state) are shown on Figure B1a′. For the case $D_o < 0$ (Figure B1b), steady state is unstable. Moreover, any solution trajectory from an initially perturbed state characterized by positive slip rate (shaded domain of Figures B1b and B1b′) evolves to either unbounded ($\Pi = \Pi_D$) or zero slip rate ($\Pi = \Pi_N(\Theta)$). It is interesting to note that under conditions of rapid drainage considered here, $\epsilon \ll 1$, the finite $O(1)$ perturbations from the steady state with positive slip rate, which are the only physically admissible ones, correspond to $\Pi < 0$ (see shaded domain on Figure B1a) in the case when the steady state is stable, $D_o > 0$, and to $\Pi > 0$ (see shaded domain on Figure B1b) in the case when the steady state is unstable, $D_o < 0$. Thus, admissible perturbations correspond to the pore fluid flow from the crustal block into the fault for stable slip and vice a versa for the eventually unstable slip. In both cases, slip evolution corresponds to increase of the dimensionless pore pressure Π, up to the zero steady state value in the former case and up to the value at instability, Π_D, in the latter case.

Appendix C: Stability Boundaries for Undrained Adiabatic Slip

[75] This appendix gives some details of the determination of the stability boundaries for undrained, adiabatic response. As discussed in the text, instability cannot occur for $\Delta > 1$. To examine the possibility of an instability for $\Delta \leq 1$, note that from (46), the inverse of dimensionless slip rate for $\Delta \leq 1$ can be written as follows

$$T_u'(\Delta) = \frac{8A}{\mu_o \mathcal{B}}\left(-\frac{a}{\mu_o \mathcal{B}} + \Delta + \frac{c}{\mu_o \mathcal{B}}\, e^{-\mu_o o \mathcal{B}\Delta}\right)$$

where the constant coefficients a and c are

$$a = 1 + \frac{\mu_o \mathcal{B}}{2} + \frac{\mu_o \mathcal{B}}{4\mathcal{A}}\left(\Phi - \frac{\mu_o \mathcal{B}}{2}\right), c = a + \frac{\mu_o^2 \mathcal{B}^2}{4\mathcal{A}}(\Phi - \Phi_{\min}) \tag{C1}$$

and $\Phi_{\min}$ is defined in (32). The solution of $T_u'(\Delta) = 0$ for $\mathcal{B} > 0$ is then given by

$$\Delta_{\text{ins}} = \frac{a + \mathrm{W}(z)}{\mu_o \mathcal{B}},\ z = -c\, e^{-a} \tag{C2}$$

where $w = \mathrm{W}(z)$ is the Lambert product log function (defined as the solution of the equation $z = we^w$). The root Δ_{ins} is real for $z \geq -e^{-1}$ (and complex otherwise). The undrained slip is *unstable* if Δ_{ins}(C2) is real and lies between 0 and 1. This will be the case only if

$$-e^{-1} \leq z \leq z_1 \tag{C3}$$

where $z = z_1$ corresponds to $\Delta_{\text{ins}} = 1$ (C2). The equations $z = -e^{-1}$ and $z = z_1$ specify the boundaries of the domain of

stable undrained slip. Note that the other boundary case $\Delta_{ins} = 0$ corresponds to $\Phi = \Phi_{min}(32)$ and, therefore, is inconsequential, because we assume, $\Phi > \Phi_{min}$, for positive initial slip rate. The upper stability domain boundary in Figure 6 corresponds to $\Delta_{ins} = 1$ (or $z = z_1$) and the lower to $z = -e^{-1}$.

[76] **Acknowledgments.** This work was supported by the National Science Foundation under grant EAR-9526767 and the U.S. Department of Energy, Office of Basic Energy Sciences under grant DE-FG02-93ER14344. JWR also wishes to acknowledge the help of Kurt Smith in making some numerical calculations early in this study.

References

Blanpied, M. L., D. A. Lockner, and J. D. Byerlee, An earthquake mechanism based on rapid sealing of faults, *Nature*, *358*, 574–576, 1992.

Brace, W. F., and R. J. Martin III, A test of the law of effective stress for crystalline rocks of low porosity, *Int. J. Rock Mech. Min. Sci.*, *5*, 415–426, 1968.

Byerlee, J., Friction, overpressure and fault normal compression, *Geophys. Res. Lett.*, *17*, 2109–2112, 1990.

Byerlee, J., Model for episodic flow of high-pressure water in fault zones before earthquakes, *Geology*, *21*, 303–306, 1993.

Cardwell, R. K., D. S. Chinn, G. F. Moore, and D. L. Turcotte, Frictional heating on a fault zone with finite thickness, *Geophys. J. R. Astron. Soc.*, *52*, 525–530, 1978.

Chambon, G., and J. W. Rudnicki, Effects of normal stress variations on frictional stability of a fluid-infiltrated fault, *J. Geophys. Res.*, *106*, 11,353–11,372, 2001.

Chester, F. M., J. P. Evans, and R. L. Biegel, Internal structure and weakening mechanisms of the San Andreas fault, *J. Geophys. Res.*, *98*, 771–786, 1993.

Coussy, O., *Mechanics of Porous Continua*, John Wiley, New York, 1995.

Detournay, E., and A. H.-D. Cheng, Fundamentals of poroelasticity, in *Comprehensive Rock Engineering*, vol. 2, chap. 5, pp. 113–171, Pergamon, New York, 1993.

Henyey, T. L., and G. L. Wasserburg, Heat flow near major strike-slip faults in California, *J. Geophys. Res.*, *76*, 7924–7946, 1971.

Lachenbruch, A. H., Frictional heating, fluid pressure, and the resistance to fault motion, *J. Geophys. Res.*, *85*, 6097–6112, 1980.

Lachenbruch, A. H., and J. H. Sass, Thermo-mechanical aspects of the San Andreas, in *Proceedings of Conference on the Tectonic Problems of the San Andreas Fault System*, edited by R. Kovach and A. Nur, pp. 192–205, Stanford Univ. Press, Palo Alto, Calif., 1973.

Lockner, D. A., and J. D. Byerlee, Dilatancy in hydraulically isolated faults and the suppression of instability, *Geophys. Res. Lett.*, *21*, 2353–2356, 1994.

Marone, C., and B. Kilgore, Scaling of the critical slip distance for seismic faulting with shear strain in fault zones, *Nature*, *362*, 618–621, 1993.

Marone, C., C. B. Raleigh, and C. H. Scholz, Frictional behavior and constitutive modeling of simulated fault gouge, *J. Geophys. Res.*, *95*, 7007–7025, 1990.

Martin, R. J., III, Pore pressure stabilization of failure in Westerly granite, *Geophys. Res. Lett.*, *7*, 404–406, 1980.

Mase, C. W., and L. Smith, Effects of frictional heating on the thermal, hydrologic, and mechanical response of a fault, *J. Geophys. Res.*, *92*, 6249–6272, 1987.

McTigue, D., Thermoelastic response of fluid-saturated porous rock, *J. Geophys. Res.*, *91*, 9533–9542, 1986.

Raleigh, C. B., and J. Evernden, Case for low deviatoric stress in the lithosphere, in *Mechanical Behavior of Crustal Rocks, Geophys. Monogr. Ser.*, vol. 24, pp. 173–186, AGU, Washington, D. C., 1981.

Raleigh, C. B., J. H. Healy, and J. D. Bredehoeft, An experiment in earthquake control at Rangely, Colorado, *Science*, *191*, 1230–1237, 1976.

Rice, J. R., Fault stress states, pore pressure distributions, and the weakness of the San Andreas fault, in *Fault Mechanics and Transport Properties of Rock: A Festschrift in Honor of W. F. Brace*, edited by B. Evans and T.-F. Wong, pp. 475–503, Academic, San Diego, Calif., 1992.

Rice, J. R., Spatio-temporal complexity of slip on a fault, *J. Geophys. Res.*, *98*, 9885–9907, 1993.

Rice, J. R., and M. P. Cleary, Some basic stress diffusion solutions for fluid-saturated elastic porous media with compressible constituents, *Rev. Geophys. Space Phys.*, *14*, 227–241, 1976.

Rudnicki, J. W., and C.-H. Chen, Stabilization of rapid frictional slip on a weakening fault by dilatant hardening, *J. Geophys. Res.*, *93*, 4745–4757, 1988.

Segall, P., and J. R. Rice, Dilatancy, compaction, and slip instability of a fluid-infiltrated fault, *J. Geophys. Res.*, *100*, 22,155–22,171, 1995.

Shaw, B. E., Frictional weakening and slip complexity in earthquake faults, *J. Geophys. Res.*, *100*, 18,239–18,251, 1995.

Sibson, R. H., Fluid flow accompanying faulting: Field evidence and models, in *Earthquake Prediction: An International Review, Maurice Ewing Ser.*, vol. 4, pp. 593–603, AGU, Washington, D. C., 1981.

Sibson, R. H., Fault zone models, heat flow, and the depth distribution of earthquakes in the continental crust of the United States, *Bull. Seismol. Soc. Am.*, *72*, 151–163, 1982.

Sibson, R. H., Continental fault structure and the shallow earthquake source, *J. Geol. Soc. London*, *140*, 741–767, 1983.

Sibson, R. H., Earthquake rupturing as a mineralizing agent in hydrothermal systems, *Geology*, *15*, 701–794, 1987.

Sibson, R. H., High angle reverse faults, fluid-pressure cycling and mesothermal gold-quartz deposits, *Geology*, *16*, 551–555, 1988.

Sibson, R. H., Loading of faults to failure, *Bull. Seismol. Soc. Am.*, *81*, 2493–2497, 1991.

Sleep, N. H., Frictional heating and the stability of rate and state dependent frictional sliding, *Geophys. Res. Lett.*, *22*, 2785–2788, 1995.

Sleep, N. H., and M. Blanpied, Creep, compaction and the weak rheology of major faults, *Nature*, *359*, 687–692, 1992.

Teufel, L. W., Pore volume changes during frictional sliding of simulated faults, in *Mechanical Behavior of Crustal Rocks, Geophys. Monogr. Ser.*, vol. 24, pp. 135–145, AGU, Washington, D. C., 1981.

Tse, S., and J. Rice, Crustal earthquake instability in relation to the depth variation of slip properties, *J. Geophys. Res.*, *91*, 9452–9472, 1986.

Vardoulakis, I., Catastrophic landslides due to frictional heating of the failure plane, *Mech. Cohes.-Frict. Mater.*, *5*, 443–467, 2000.

Wagner, W., and A. Kruse, *Properties of Water and Steam*, Springer-Verlag, New York, 1998.

D. I. Garagash, Department of Civil and Environmental Engineering, Clarkson University, Potsdam, NY 13699-5710, USA. (garagash@clarkson.edu)

J. W. Rudnicki, Department of Civil and Environmental Engineering, Northwestern University, Evanston, IL 60208, USA. (jwrudn@nwu.edu)